PHOTONIC CRYSTAL FIBER BASED OPTICAL FIBER CORE DESIGN FOR SENSING AND TRANSMISSION IN TERAHERTZ SPECTRUM

By

Shazedul Islam (142450)

Abu Nahid Saroar (142452)

Khandoker Md. Abu Talha (142477)

Mushfiqur Rahman (142488)

A Thesis Submitted to the Academic Faculty in Partial Fulfillment of the Requirements for the Degree of

BACHELOR OF SCIENCE IN ELECTRICAL AND ELECTRONIC ENGINEERING

Department of Electrical and Electronic Engineering

Islamic University of Technology (IUT)

Gazipur, Bangladesh

November 2018

PHOTONIC CRYSTAL FIBER BASED OPTICAL FIBER CORE DESIGN FOR SENSING AND TRANSMISSION IN TERAHERTZ SPECTRUM

Approved by:

Prof Dr. Md. Rakibul Islam (Supervisor)

Department of Electrical and Electronic Engineering,

Islamic University of Technology (IUT),

Boardbazar, Gazipur-1704

Date:

Prof. Dr. Md. Ashraful Hoque

Head,

Department of Electrical and Electronic Engineering,

Islamic University of Technology (IUT),

Boardbazar, Gazipur-1704

Date:

TABLE OF CONTENTS

2 EVOLUTION OF OPTICAL FIBER

3 PHOTONIC CRYSTAL FIBER AND THz BAND

6 BACKGROUND MATERIALS

7 FACTOR AND LOSSES IN OPTICAL FIBER

ACKNOWLEDGEMENTS

The first thank and honor go to the Almighty. He has given us the capability and Opportunity to finish this work perfectly. We have tried our best through the whole year and this research is our most significant scientific accomplishment in our educational life. But, without His help, it would not be possible for us.

After that, we would like to thank our honorable respective supervisor, Prof. Dr. Mohammad Rakibul Islam for his guidance, motivation and help during the thesis work. He has worked very hard and helped us a lot to finish and finalize this research work.

We would also like to thank other respective teachers, our friends and family members for their support and motivation which were also the key points behind our success.

ABSTRACT

Terahertz radiation occupies a middle ground between microwaves and infrared light waves known as the terahertz gap, where technology for its generation and manipulation is in its infancy. The frequency band of 0.1-10 THz, known as THz band has brought potential applications in many important fields. For wave propagation THz systems use free space as medium. But in free space waves face many difficulties which is very big issue for wave propagation. So we have to use guided transmission instead of unguided transmission. In the meantime many guided transmission line has many kinds of deprivation such as effective material loss, confinement loss, bending loss, dispersion loss, power fraction issue etc. So we had decided to make a hollow core porous core fiber which has less losses than other PCF. Mainly we have been inspired from previous papers in which these losses was too much high for THz wave guidance.

Then we have designed a novel hollow core photonic crystal fiber (PCF) which consists of symmetrical hexagonal rings in its cladding distributed in three rows. The prime objective of this work is to increase the sensitivity but other significant features like effective material loss, confinement loss, effective area, numerical aperture and dispersion have been thoroughly investigated over a wide bandwidth using the finite element method-based commercially available software, COMSOL version 5.3. Numerical simulation shows that, a maximum chemical sensitivity of 99.39%, 99.76% and 99.44% can be obtained for methanol, benzene and water respectively at optimum operating conditions. The symmetry in design makes the proposed structure easily feasible to be fabricated using the existing fabrication technologies. Thus it is believed that the proposed PCF has the potential to uplift the standard of photonic crystal fiber sensors and open a new window in this field of research.

CHAPTER 1

AN OVERVIEW OF OPTICAL FIBER COMMUNICATION

1.1 Optical Fiber Communication

Fiber optic communication is a communication technology that uses light pulses to transfer information from one point to another through an optical fiber. The information transmitted is essentially digital information generated by telephone systems, cable television companies, and computer systems.

1.2 Evolution of Optical Fiber Communication

1.2.1 Background

Optical fiber was first developed in 1970 by Corning Glass Works. At the same time, GaAs semiconductor lasers were also developed for transmitting light through the fiber optic cables. The first generation fiber optic system was developed in 1975, it used GaAs semiconductor lasers, operated at a wavelength of 0.8 μm, and bit rate of 45Megabits/second with 10Km repeater spacing.

In the early 1980's, the second generation of fiber optic communication was developed, it used InGaAsP semiconductor lasers and operated at a wavelength of 1.3 μm.

By 1987, these fiber optic systems were operating at bit rates of up to 1.7 Gigabits/second on single mode fiber with 50Km repeater spacing.

1.2.2 3rd Generation

The third generation of fiber optic communication operating at a wavelength of 1.55 μm was developed in 1990. These systems were operating at a bit rate of up to 2.5 Gigabits/second on a single longitudinal mode fiber with 100Km repeater spacing.

1.2.3 4th Generation

The fourth generation of fiber optic systems made use of optical amplifiers as a replacement for repeaters, and utilized wavelength division multiplexing (WDM) to increase data rates. By 1996, transmission of over 11,300Km at a data rate of 5Gigabits/second had been demonstrated using submarine cables.

1.2.4 5th Generation

The fifth generation fiber optic communication systems use the Dense Wave Division Multiplexing (DWDM) to further increase data rates. Also, the concept of optical solitons, which are pulses that can preserve their shape by counteracting the negative effects of dispersion, is also being explored.

1.3 Ingredients

The major driving force behind the widespread use of fiber optics communication is the high and rapidly increasing consumer and commercial demand for more telecommunication capacity and internet services, with fiber optic technology capable of providing the required information capacity (larger than both wireless

connections and copper cable). Advances in technology have enabled more data to be conveyed through a single optical fiber over long distances. The transmission capacity in optical communication networks are significantly improved using wavelength division multiplexing.

1.4 Mechanism

An optical network has the ability to process information entirely in the optical domain for the purpose of amplification, multiplexing, de-multiplexing, switching, filtering, and correlation, since optical signal processing is more efficient than electrical signal processing. Code Division Multiple Access networks using optical signal processing techniques have recently being introduced.

1.5 Optical Fiber Waveguide

An optical fiber is a dielectric cylindrical waveguide made from low-loss materials, usually silicon dioxide. The core of the waveguide has a refractive index a little higher than that of the outer medium (cladding), so that light pulses is guided along the axis of the fiber by total internal reflection.

1.6 Transmission Through Fiber

Fiber optic communication systems consists of an optical transmitter to convert an electrical signal to an optical signal for transmission through the optical fiber, a cable containing several bundles of optical fibers, optical amplifiers to boost the power of

the optical signal, and an optical receiver to reconvert the received optical signal back to the original transmitted electrical signal.

1.7 Basic Optical Fiber Communication

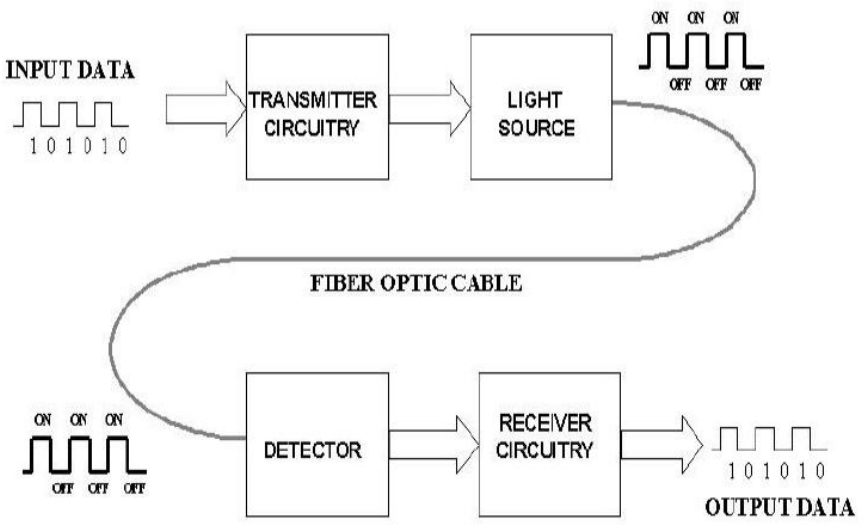

Fig 1.1: Basic fiber optic communication system

Figure 1.1 gives a simplified description of a basic fiber optic communication system Fiber-optic communication is a method of transmitting information from one place to another by sending pulses of light through an optical fiber. The light forms an electromagnetic carrier wave that is modulated to carry information. Fiber is preferred over electrical cabling when high bandwidth, long distance, or immunity to electromagnetic interference are required. Optical fiber is used by many

telecommunications companies to transmit telephone signals, Internet communication, and cable television signals

1.8 Categories of Optical Fiber

Optical fibers fall into two major categories, namely:

- Step index optical fiber
- Graded index optical fiber

1.8.1 Step Index Optical Fiber

Step index optical fiber, which include single mode optical fiber and multimode optical fiber, and graded index optical fiber. Single mode step index optical fiber has a core diameter less than 10 micrometers and only allows one light path. Multimode step index optical fiber has a core diameter greater than or equal to 50 micrometers and allows several light paths, this leads to modal dispersion.

1.8.2 Graded Index Optical Fiber

Graded index optical fibers have their core refractive index gradually decrease farther from the center of the core, this increased refraction at the core center slows the speed of some light rays, thereby allowing all the light rays to reach the receiver at almost the same time, thereby reducing dispersion.

1.9 Various Categories Fiber Mode

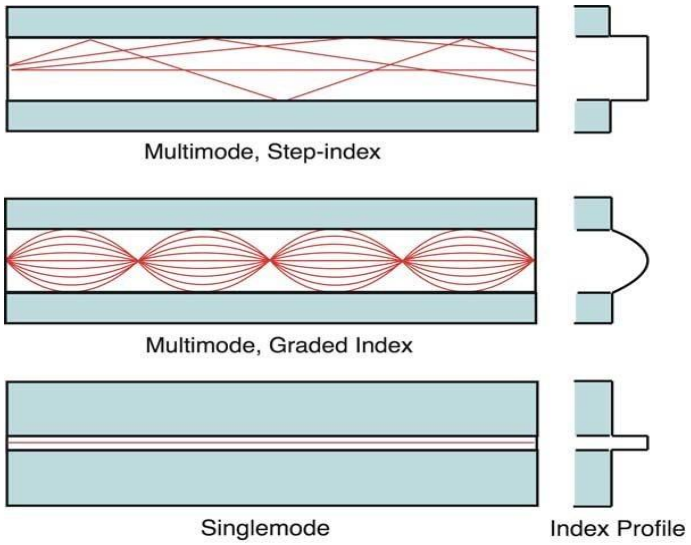

Fig 1.2: Optical Fiber Modes

Figure 1.2 gives a description of the various optical fiber modes. Single mode optical fiber transmits only one mode of light. Multimode optical fibers allow multiple modes of light to travel along their axis. In case of Stepped index multimode fiber the refractive index of the core of the multimode is uniform throughout the cable. And for graded index multimode fiber the refractive index of the core changes radially from the center of the core to its surface.

1.10 Basic Steps

The process of communicating using fiber-optics involves the following basic steps:

1. Creating the optical signal involving the use of a transmitter, usually from an electrical signal.

2. Relaying the signal along the fiber, ensuring that the signal does not become too distorted or weak

3. Receiving the optical signal

4. Converting it into an electrical signal

1.11 Technology

Modern fiber-optic communication systems generally include an optical transmitter to convert an electrical signal into an optical signal to send into the optical fiber, a cable containing bundles of multiple optical fibers that is routed through underground conduits and buildings, multiple kinds of amplifiers, and an optical receiver to recover the signal as an electrical signal. The information transmitted is typically digital information generated by computers, telephone systems, and cable television companies.

1.12 Transmitters

The most commonly used optical transmitters are semiconductor devices such as light-emitting diodes (LEDs) and laser diodes. The difference between LEDs and laser diodes is that LEDs produce incoherent light, while laser diodes produce coherent light. For use in optical communications, semiconductor optical transmitters must be designed to be compact, efficient, and reliable, while operating in an optimal wavelength range, and directly modulated at high frequencies.

1.13 LED

In its simplest form, an LED is a forward-biased p-n junction, emitting light through spontaneous emission, a phenomenon referred to as electroluminescence. The emitted light is incoherent with a relatively wide spectral width of 30-60 nm. LED light transmission is also inefficient, with only about 1% of input power, or about 100 microwatts, eventually converted into launched power which has been coupled into the optical fiber. However, due to their relatively simple design, LEDs are very useful for low-cost applications. Today, LEDs have been largely superseded by VCSEL (Vertical Cavity Surface Emitting Laser) devices, which offer improved speed, power and spectral properties, at a similar cost. Common VCSEL devices couple well to multimode fiber.

1.14 Receivers

The main component of an optical receiver is a photodetector, which converts light into electricity using the photoelectric effect. The primary photodetectors for telecommunications are made from Indium gallium arsenide. The photo detector is typically a semiconductor-based photodiode. Several types of photodiodes include p-n photodiodes, p-i-n photodiodes, and avalanche photodiodes. Metal-semiconductor-metal (MSM) photo detectors are also used due to their suitability for circuit integration in regenerators and wavelength-division multiplexers.

Optical-electrical converters are typically coupled with a trans-impedance amplifier and a limiting amplifier to produce a digital signal in the electrical domain from the incoming optical signal, which may be attenuated and distorted while passing through the channel. Further signal processing such as clock recovery from data

(CDR) performed by a phase-locked loop may also be applied before the data is passed on.

1.15 Transceiver

A transceiver is a device combining a transmitter and a receiver in a single housing. Most systems use a "transceiver" which includes both transmission and receiver in a single module. The transmitter takes an electrical input and converts it to an optical output from a laser diode or LED. The light from the transmitter is coupled into the fiber with a connector and is transmitted through the fiber optic cable plant. The light from the end of the fiber is coupled to a receiver where a detector converts the light into an electrical signal which is then conditioned properly for use by the receiving equipment.

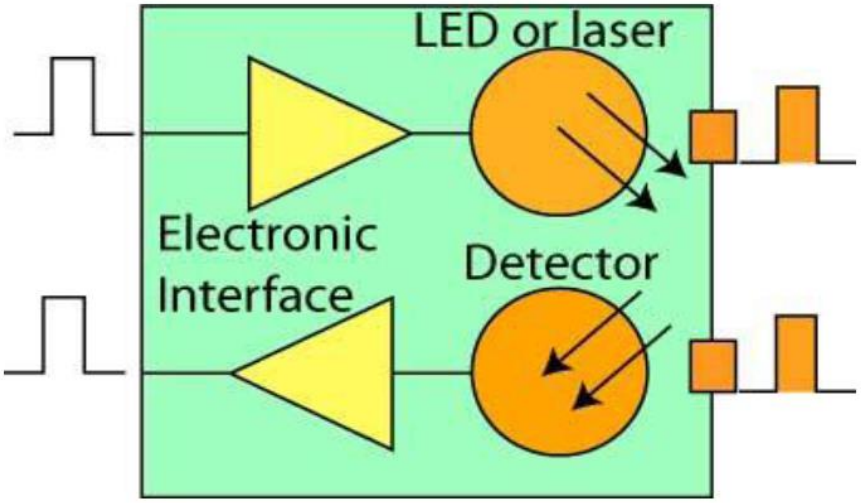

Fig 1.3: Fiber Optic Transceiver

1.16 Amplifier

The transmission distance of a fiber-optic communication system has traditionally been limited by fiber attenuation and by fiber distortion. By using opto-electronic repeaters, these problems have been eliminated. These repeaters convert the signal into an electrical signal, and then use a transmitter to send the signal again at a higher intensity than was received, thus counteracting the loss incurred in the previous segment. Because of the high complexity with modern wavelength-division multiplexed signals (including the fact that they had to be installed about once every 20 km), the cost of these repeaters is very high.

1.17 Wavelength-Division Multiplexing

Wavelength-division multiplexing (WDM) is the practice of multiplying the available capacity of optical fibers through use of parallel channels, each channel on a dedicated wavelength of light. This requires a wavelength division multiplexer in the transmitting equipment and a demultiplexer (essentially a spectrometer) in the receiving equipment. Arrayed waveguide gratings are commonly used for multiplexing and demultiplexing in WDM. Using WDM technology now commercially available, the bandwidth of a fiber can be divided into as many as 160 channels to support a combined bit rate in the range of 1.6Tbit/s.

1.18 Applications

Optical fiber is used by many telecommunications companies to transmit telephone signals, Internet communication, and cable television signals. Due to much lower attenuation and interference, optical fiber has large advantages over existing copper wire in long-distance and high-demand applications. However, infrastructure development within cities was relatively difficult and time-consuming, and fiber-optic systems were complex and expensive to install and operate. Due to these difficulties, fiber-optic communication systems have primarily been installed in long-distance applications, where they can be used to their full transmission capacity, offsetting the increased cost. Since 2000, the prices for fiber-optic communications have dropped considerably.

CHAPTER 2

EVOLOUTION OF OPTICAL FIBER

In the recent years THz wave generation and detection techniques have already been developed to cope with its popularity. However due to the lack of low loss transmission waveguides in the THz frequencies, most of the THz systems depends on free space for its wave propagation since all the remaining waveguides are extremely absorbent in this frequency band. Propagation in free space faces some undesirable problems. These include a tough configuration, path loss, an uncertain absorption loss influenced by the atmosphere, and difficult integration with other components. Therefore, transmissions of THz waves for long distance are still in the demanding state.

Therefore much effort has been given for its solutions, one can be to use optical fiber where there is no influence of external free space, these can dramatically reduce the losses and alignment problems also the system performances can also be increased.

2.1 Introduction to Terahertz

The TERAHERTZ (THz) frequency/wavelength window of the electro-magnetic spectrum lies between the infrared band and the microwave band and ranges in frequency from 0.1 to 10 THz (equivalently wavelength ranges from 3 mm – 30 μm). Radiation from any object with temperature > 10 K contains THz wavelengths and almost 98% of cosmic background radiations since Big-Bang event corresponds to THz and far-infrared frequencies. Initially THz radiation was mainly used for passive

Applications, where THz waves were detected to study the chemistry of cold planetary atmosphere and interstellar medium.

2.1.1 Why Researchers Decided To Use This Gap

This frequency range can transfer huge data files via wireless route and can significantly increase the communication data rate over existing microwave technology. THz waves can deeply penetrate through cloths, ceramics, walls, woods, paper, dry air, polymers etc., but they are absorbed or reflected by metal, water vapor, dust, cloud, and sufficiently dense objects. Additionally, THz waves are also not harmful to human health. All these excellent qualities of THz radiation make it suitable for imaging of hidden objects, like explosives, metallic weapons etc. Most importantly, this technology has already begun to make deep inroads in non-invasive medical diagnostics, such as detection of skin cancer, tooth decay, and identification of human tissues based on different refractive indices and linear absorption coefficients at THz frequencies.

2.2 Wave Propagation

Since most of the THz systems and THz communication experiments are bulky and are performed in free space, it faces many undesirable problems. These include a tough transmitter-receiver alignment issues, an uncertain absorption loss influenced by the surroundings and difficult integration with other components.

2.2.1 Guided Transmission

To overcome these problems, researchers proposed guided transmission instead of unguided transmission. Researchers showed that the THz wave can nicely be propagated through all kinds of conventional metallic waveguides.

2.3 Background of THz Waveguides

2.3.1 Auston Switch

In the early 1980s, THz pulses (in the Pico/sub picosecond regime) were generated and sampled by photoconductive switches, also known as Auston switches. These photoconductive switches were incorporated into micro strip and coplanar (still used today) transmission lines.

2.3.2 Microstrip

A micro strip transmission line is a type of electrical transmission line that consists of a conducting strip separated from a ground plane by a dielectric substrate, while a coplanar transmission line is an alternative type of electrical transmission line that consists of a conducting strip on a dielectric substrate with two ground electrodes running adjacent and parallel to strip.

2.3.3 Limitation of Microstrip

A limitation of the microstrip line configuration, in the THz system, was that such systems suffered from reflections (ringing) at the generation point. Also these microstrip based THz systems had high dispersion due to the dielectric substrate.

2.3.4 Coplanar

In the coplanar transmission THz system, the generated sub picosecond pulse (0.6 ps, for example) undergoes lower distortion compared to microstrip lines. Therefore, they are more suitable for far-IR spectroscopy.

2.3.5 Limitation of Coplanar

The coplanar transmission line THz system suffers from strong frequency dependent loss due to Cherenkov-like radiation, which is equivalent to the loss process of leaky waveguides in the frequency domain. The total observed loss owing to the dielectric and metal in microstrip and coplanar transmission lines in THz systems is very high.

2.3.6 Reported Losses

For thin-film microstrip and coplanar transmission lines are $\alpha = 18$ cm-1 and $\alpha = 14$ cm-1 at 1 THz, respectively. The loss increases as frequency increases with f and f3 dependence, respectively.

2.3.7 Circular Metallic Waveguide

Initially, to propagate THz wave researchers used Circular metallic waveguide like stainless solid but these waveguide are highly lossy on the order of 50 DB/cm. Although a THz wave cannot be guided inside a hollow dielectric tube, if this tube is coated with a metal layer, a plasmonic mode can form inside the hollow core, where the guiding environment can be better controlled or manipulated.

2.3.8 Additional Thin Dielectric Layer

It has been observed that by incorporating an additional thin dielectric layer the mode field can be drawn away from the lossy plasmonic interface and, as a consequence, the overall loss value can be reduced. However, these waveguides are not very flexible for large diameter waveguides and increase the loss value for small diameter waveguides.

2.3.9 Hollow Core Fiber

Hollow dielectric tubes coated with metal layer were reported, but they appeared to be bulky in the design but they showed us larger core power fraction. And they also showed us lower effective material loss as there is low amount of material in the core.

2.3.10 Low Index Dry Index

To overcome these obstacles, one usually designs various kinds of waveguides to guide the THz wave because the material absorption loss is high in THz band. One of the lowest material loss materials is dry air in the THz frequency range. It has been reported that the mode field extends into the low index air cladding region when a dielectric rod is surrounded by air and is operating very close to its cutoff frequency. The main disadvantage of this design is that the mode extends considerably into the surrounding air cladding and the power is propagated mostly outside the waveguide, which strongly interacts with the surrounding environment. As a result, the bending loss would also be expected to be excessively high.

2.3.11 Plastic Sub wavelength Fibers

Plastic sub wavelength fibers came into existence for their comparatively lower losses. However, there is a disadvantage for the sub-wavelength fibers that most of the field propagates outside the waveguide core, thus resulting in strong coupling to the environment.

For improvement, Nagel et al. Reported the addition of a sub-wavelength hole within a solid core, which increases the guided field in the air hole and hence reducing the absorption losses. However, the loss due to the material is still high.

2.4 Use of Polymers

Interest of researchers shifted from dielectrics to polymers when Chen et al. showed that polyethylene can be used as a guidance material which has lower absorption

loss. In recent times, variety of polymers such as Polymethyl Methacrylate (PMMA) TOPAS Teflon etc. are being used as primary choices for THz wave guiding.

In order to reduce absorption loss further, researchers put their attention into guiding structure designing. Dry air is assumed to have no material absorption loss at THz frequency range. On the basis of that, wave guide with sub-wavelength air hole in the core was reported .However, it caused huge power dissipation outside the guide. Later, polystyrene foam was introduced which had a major disadvantage that it required larger dimension.

Actually, genuine breakthrough of the research works occurred when polymer materials were used instead of metals in the background which represent a much lower absorption loss.

2.4.1 Hollow core Bragg Fiber

Hollow core Bragg fibers have also been considered which, unfortunately, had unwanted narrow band properties.

2.4.2 Photonic Crystal Fiber

Photonic crystal fiber (PCF) is the most popular optical fiber but in case of a solid core the material absorption loss is too high and is almost equal to the bulk absorption loss of the material.

In a PCF, light is guided through the waveguide using total internal reflection property based on the difference between refractive indices of the core and the cladding. In general, the cladding is consisted of a number of air holes. Recently,

PCFs have been popular for their modification enabled property which helps controlling their behavior. Although, solid core polymer-made PCFs had been introduced for THz wave guiding they could not create a spark because the solid core caused significant amount of loss. As an attempt, air filling ratio was extremely increased to force the light through air holes of the cladding but size of the waveguide got enlarged.

2.5 Use of Porous Air Core in PCF

Implementing porous air core in a PCF instead of solid rod came out as a solution. Use of a porous core is resulted in reduction of quantity of solid material in the core as well as the absorption loss.

2.5.1 Honeycomb Band-gap Fibers

Efficient honeycomb band-gap fibers were reported where porous core PCFs were investigated both numerically and experimentally. Also, a hexagonal PCF with hexagonal porous core was reported with a low absorption loss (0.12 cm-1) where Teflon was used as the background material.

2.5.2 Sub-wavelength Porous Fibers

The sub-wavelength porous fibers have been proven to exhibit some merits namely extremely low loss, design and fabrication flexibilities, and small fiber diameters. Moreover, dispersion of the porous fibers can be controlled easily. In such fibers,

owing to the sub-wavelength diameter of the core, the fundamental guided mode presents surrounding the air-cladding and hence low absorption loss is obtained.

2.5.3 Use of ZEONEX

A better approach with ZEONEX was presented which had an octagonal porous core inside an octagonal cladding with a lower loss (0.07 cm-1) resulted due to the lower

Bulk material absorption loss of ZEONEX. Nevertheless, the paper had no discussion on power fraction or dispersion properties

CHAPTER 3

PHOTONIC CRYSTAL FIBER AND THz BAND

3.1 Photonic Crystal Fiber

Photonic-crystal fiber (PCF) is a new class of optical fiber based on the properties of photonic crystals. Because of its ability to confine light in hollow cores or with confinement characteristics not possible in conventional optical fiber, PCF is now finding applications in fiber-optic communications, fiber lasers, nonlinear devices, high-power transmission, highly sensitive gas sensors, and other areas. More specific categories of PCF include photonic-bandgap fiber (PCFs that confine light by band gap effects), holey fiber (PCFs using air holes in their cross-sections), hole-assisted fiber (PCFs guiding light by a conventional higher-index core modified by the presence of air holes), and Bragg fiber (photonic-bandgap fiber formed by concentric rings of multilayer film). Photonic crystal fibers may be considered a subgroup of a more general class of micro-structured optical fibers, where light is guided by structural modifications, and not only by refractive index differences.

3.1.1 Description

Optical fibers have evolved into many forms since the practical breakthroughs that saw their wider introduction in the 1970s as conventional step index fibers and later as single material fibers where propagation was defined by an effective air cladding structure.

In general, regular structured fibers such as photonic crystal fibers, have a cross-section (normally uniform along the fiber length) micro-structured from one, two or more materials, most commonly arranged periodically over much of the cross-section, usually as a "cladding" surrounding a core (or several cores) where light is confined. For example, the fibers first demonstrated by Russell consisted of a hexagonal lattice of air holes in a silica fiber, with a solid (1996) or hollow (1998) core at the center where light is guided. Other arrangements include concentric rings of two or more materials, first proposed as "Bragg fibers" by Yeh and Yariv (1978), a variant of which was recently fabricated by Temelkuranet al. (2002) and others. (Note: PCFs and, in particular, Bragg fibers, should not be confused with fiber Bragg gratings, which consist of a periodic refractive index or structural variation along the fiber axis, as opposed to variations in the transverse directions as in PCF. Both PCFs and fiber Bragg gratings employ Bragg diffraction phenomena, albeit in different directions.)

The lowest reported attenuation of solid core photonic crystal fiber is 0.37 dB/km, and for hollow core is 1.2 dB/km.

3.1.2 Construction

Generally, such fibers are constructed by the same methods as other optical fibers: first, one constructs a "preform" on the scale of centimeters in size, and then heats the preform and draws it down to a much smaller diameter (often nearly as small as a human hair), shrinking the preform cross section but (usually) maintaining the same features. In this way, kilometers of fiber can be produced from a single preform. The most common method involves stacking, although drilling/milling was

used to produce the first aperiodic designs. This formed the subsequent basis for producing the first soft glass and polymer structured fibers.

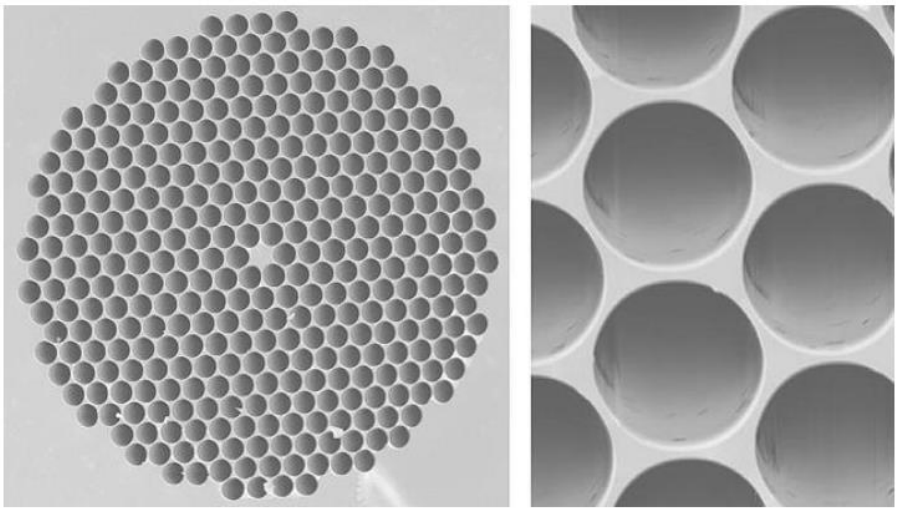

Fig 4.1: Photonic Crystal Fiber

Most photonic crystal fibers have been fabricated in silica glass, but other glasses have also been used to obtain particular optical properties (such as high optical non-linearity). There is also a growing interest in making them from polymer, where a wide variety of structures have been explored, including graded index structures, ring structured fibers and hollow core fibers. These polymer fibers have been termed "MPOF", short for micro-structured polymer optical fibers (van Eijkelenborg, 2001). A combination of a polymer and a chalcogenide glass was used by Temelkuranet al. (2002) for 10.6 μm wavelengths (where silica is not transparent).

3.1.3 Modes of Operation

Photonic crystal fibers can be divided into two modes of operation, according to their mechanism for confinement. Those with a solid core, or a core with a higher average index than the micro-structured cladding, can operate on the same index-guiding principle as conventional optical fiber — however, they can have a much higher effective- refractive index contrast between core and cladding, and therefore can have much stronger confinement for applications in nonlinear optical devices, polarization-maintaining fibers, (or they can also be made with much lower effective index contrast). Alternatively, one can create a "photonic bandgap" fiber, in which the light is confined by a photonic bandgap created by the micro-structured cladding – such a bandgap, properly designed, can confine light in a lower-index core and even a hollow (air) core. Bandgap fibers with hollow cores can potentially circumvent limits imposed by available materials, for example to create fibers that guide light in wavelengths for which transparent materials are not available (because the light is primarily in the air, not in the solid materials). Another potential advantage of a hollow core is that one can dynamically introduce materials into the core, such as a gas that is to be analyzed for the presence of some substance. PCF can also be modified by coating the holes with sol-gels of similar or different index material to enhance its transmittance of light.

3.2 THz Band and Its Application

Terahertz radiation falls in between infrared radiation and microwave radiation in the electromagnetic spectrum and it shares some properties with each of these. Like infrared and microwave radiation, terahertz radiation travels in a line of sight and is non-ionizing. Like microwave radiation, terahertz radiation can penetrate a wide

variety of non-conducting materials. Terahertz radiation can pass through clothing, paper, cardboard, wood, masonry, plastic and ceramics. The penetration depth is typically less than that of microwave radiation. Terahertz radiation has limited penetration through fog and clouds and cannot penetrate liquid water or metal. In physics, terahertz radiation, also called submillimeter radiation, terahertz waves, terahertz light, T-rays, T-waves, T-light, T-lux, or THz, consists of electromagnetic waves at frequencies from 0.3 to 10 terahertz (THz). The term applies to electromagnetic radiation with frequencies between the high-frequency edge of the millimeter wave band, 300 GHz and the low frequency edge of the far-infrared light band, 3000 GHz. Corresponding wavelengths of radiation in this band range from 1 mm to 0.1 mm (or 100 μm). Because terahertz radiation begins at a wavelength of 1 mm and proceeds into shorter wavelengths, it is sometimes known as the submillimeter band and its radiation as submillimeter waves, especially in astronomy.

The earth's atmosphere is a strong absorber of terahertz radiation in specific water vapor absorption bands, as seen in Fig. 1, so the range of terahertz radiation is limited enough to affect its usefulness in long-distance communications. However, at distances of ∼10 m the band may still allow many useful applications in imaging and construction of high bandwidth wireless networking systems, especially indoor systems.3 In addition, producing and detecting coherent terahertz radiation remains technically challenging, though inexpensive commercial sources now exist in the 300–1000 GHz range (the lower part of the spectrum), including gyrotrons, backward wave oscillators, and resonant-tunneling diodes.

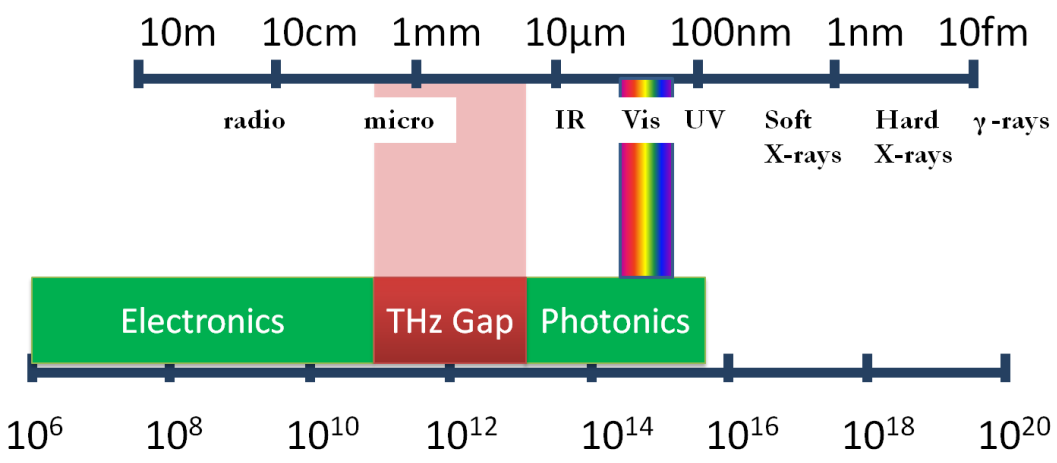

Fig 4.2: THz gap in electromagnetic spectrum

Terahertz radiation occupies a middle ground between microwaves and infrared light waves, and technology for generating and manipulating it is in its infancy and is a subject of active research (Fig. 1). It represents the region in the electromagnetic spectrum in which the frequency of electromagnetic radiation becomes too high to be measured by directly counting cycles using electronic counters, and must be measured by the proxy properties of wavelength and energy.

Similarly, in this frequency range the generation and modulation of coherent electromagnetic signals ceases to be possible by the conventional electronic devices used to generate radio waves and microwaves, and requires new devices and techniques. The electromagnetic range that is used is very vast. At low frequencies end we have radio waves up to millimeter waves, and at the other end we have optical waves down to the far infrared. Technologies have been developed for both ends of the spectrum which we use in everyday applications. But the terahertz region:

0.3-10 THz, 1THz=1012Hz

With wavelength of 30 μm–3 mm has remained largely underdeveloped, despite the identification of various applications, in particular terahertz imaging and others which will be discussed later on.

It is possible to produce effectively radiation in the low frequency region (microwaves) with oscillating circuits based on high-speed transistors and at high frequencies (visible spectrum) with semiconductor lasers. But transistors and other electric devices based on electric transport have in principle a limit at about 300 GHz, but are practically limited to about 50 GHz, because devices above this are extremely inefficient and the frequency of semiconductor lasers can only be extended down to about 30 THz. Thus there is a region in between where both technologies do not meet. This region is often referred to as the terahertz gap.

Terahertz radiations have a few remarkable properties. Many common materials and living tissues are semitransparent and have 'terahertz fingerprints', permitting them to be imaged, identified and analyzed. Due to non-ionizing properties of terahertz radiations are safe for screening application. These unique properties of radiations are now exploited due to availability of commercial sources of terahertz radiations.

3.2.1 Application:

3.2.1.1 Pharmaceutical Industry: Tablet Integrity and Performance

Coating has a wide variety of functions. The most important function of coating is to regulate the controlled release of active ingredients in the body. Coating not only contributes to the bioavailability of a particular drug or combination of drugs during

certain times and locations but also coating can protect the stomach from high concentrations of active ingredients, improve tablet visual appeal and extend shelf life by protecting the ingredients from degradation by moisture and oxygen. In relation to tablet coating the process analytical technology (PAT) initiative is intended to improve consistency and predictability of tablet action by improving quality and uniformity of tablet coatings. Issues with coating can arise from problems with the coating materials or flaws in the coating pan or spray process. If a coating is non-uniform or has surface defects then the desired dose delivery and bioavailability can be compromised. From this standpoint it is important to characterize tablet coating uniformity, both within a single tablet and across an entire batch to develop an understanding of the functional analysis of the final product. Several analytical and imaging techniques are being used to understand the critical processes involved in tablet coating but none of them is ideal to fully characterize the layers. Some of the techniques that provide useful information are atomic force microscopy, confocal laser microscopy, X-ray photoelectron spectroscopy, electron paramagnetic resonance, Fourier transform infrared spectroscopy, and laser induced breakdown spectroscopy (LIBS) and scanning thermal microscopy. However all these methods are either destructive to the tablet or cannot be readily implemented for rapid on-line measurement.

Terahertz image can be optimized for performing 3D analysis on tablets. It can enable to determine coating integrity and thickness, detect and identify localized chemical or physical structure such as cracks or chemical agglomeration within a core and to interrogate embedded layers (such as an interface between two layers) for delamination and integrity. Terahertz measurements may well become the primary method for the nondestructive determination of coating thickness, requiring

little or no calibration for most coatings and substrates. It can reveal the thickness, uniformity, distribution and coverage of simple and complex coating. Terahertz image can also detect embedded layers and localized chemical or physical structural features in the cores of intact tablets to confirm 3D morphology and blend uniformity.

3.2.1.2 Terahertz Pulsed Imaging (TPI)

TPI is a completely non-invasive and non-destructive pharmaceutical analysis tool using extremely low power, ultra-short pulses of electromagnetic radiation at lower frequencies than infrared (1 THz = 1012 Hz).Terahertz spectroscopy has already proved useful to distinguish between different polymorph forms of the drug. TPI is a next step of this whereby THz pulses are used to image object of interest. THz pulses are generated by illuminating photoconductive semi-conductors with pulsed near-infrared laser radiation and detected coherently. Tablet coatings are semi-transparent to THz frequencies and do no scatter them significantly. THz pulses incident on a tablet surface penetrate through the different coating layers. At each interface a portion of THz radiations is reflected back to the detector. The amplitude of reflected THz radiation is recorded as a function of time. In this technique the sample itself is completely unaffected by the measurement. Coating thickness uniformity is established simply from the transit time of the pulse to each interface. With knowledge of the refractive index of coating material the actual thickness can be determined to a depth resolution of about 20 microns. The spot size of the THz pulse, and therefore lateral resolution, is about 250 microns.

3.2.1.3 Molecular Structure

The sensitivity and specificity of terahertz spectroscopy to both intermolecular and intramolecular vibrations in different chemical species enable investigation of the crystalline state of drugs e.g. Polymorphism. The use of pulsed terahertz imaging in proteomics and drug discovery determines protein 3D structure, folding and characterization. It is also very sensitive to DNA hybridization and other interactions. Terahertz spectroscopy provides rapid identification of the different crystalline forms of drug molecules – the polymorphs – which can exhibit different solubility's, stabilities and bioavailability and hence are an important factor in the therapeutic efficacy of a drug. Detecting and identifying the different polymorphs and understanding the mechanism and dynamics of polymorphic inter-conversion, is an important milestone in selecting the optimum form for further development and manufacture. It is possible not only to detect the differences between pure specimens of the polymorphs but terahertz spectroscopy can distinguish between specific polymorphic forms in tablet formulation.

Terahertz spectroscopy can also differentiate between different hydrate forms. Lactose which is one the most commonly used excipients in the pharmaceutical industry has at least three different hydrates namely α-monohydrate, α-anhydrate and β-anhydrate form. These three hydrate forms exhibit terahertz spectra that can be used for both quantitative and qualitative analysis. Terahertz region provides unique sensitivity to lattice structure enabling qualitative and qualitative analysis of crystalline and amorphous materials as well.

3.2.1.4 Security

Terahertz radiation can penetrate fabrics and plastics, so it can be used in surveillance, such as security screening, to uncover concealed weapons on a person, remotely. This is of particular interest because many materials of interest have unique spectral “fingerprints” in the terahertz range. This offers the possibility to combine spectral identification with imaging. Passive detection of terahertz signatures avoids the bodily privacy concerns of other detection by being targeted to a very specific range of materials and objects.

At airports or other security critical places dangerous non-metallic substances like ceramic knifes or plastic explosives now can be detected with terahertz beams. This is possible because T-rays get through clothes, but cannot get through the upper skin (because of the water content).

3.2.1.5 Communication

Potential uses exist in high-altitude telecommunications, above altitudes where water vapor causes signal absorption: aircraft to satellite, or satellite to satellite.

CHAPTER 4

PLATFORM: COMSOL MULTIPHYSICS VERSION 5.3

4.1 Creating a New Model

We can set up a model guided by the Model Wizard or start from a Blank Model.

4.1.1 Creating a Model Guided By the Model Wizard

The Model Wizard will guide you in setting up the space dimension, physics, and study type in a few steps:

1. Start by selecting the space dimension for your model component: 3D, 2D Axisymmetric, 2D, 1D Axisymmetric, or 0D.

2. Now, add one or more physics interfaces. These are organized in a number of Physics branches in order to make them easy to locate. These branches do not directly correspond to products. When products are added to your COMSOL Multiphysics installation, one or more branches will be populated with additional physics interfaces.

3. Select the Study type that represents the solver or set of solvers that will be used for the computation. Finally, click done. The desktop is now displayed with the model tree configured according to the choices you made in the Model Wizard.

4.1.2 Creating a Blank Model

The Blank Model option will open the COMSOL Desktop interface without any Component or Study. You can right-click the model tree to add a Component of a certain space dimension, physics interface, or Study.

4.2 Parameter, Variables and Scope

4.2.1 Global Parameters

Global parameters are user-defined constant scalars that are usable throughout the model. That is to say, they are "global" in nature. Important uses are:

• Parameterizing geometric dimensions.

• Specifying mesh element sizes.

• Defining parametric sweeps (simulations that are repeated for a variety of different values of a parameter such as a frequency or load).

A global parameter expression can contain numbers, global parameters, built-in constants, and built-in functions with global parameter expressions as arguments, and unary and binary operators.

For a list of available operators, Language Elements and Reserved Names". Because these expressions are evaluated before a simulation begins, global parameters may not depend on the time variable t. Likewise, they may not depend on spatial variables like x, y, or z, nor on the dependent variables for which your equations are solving.

It is important to know that the names of parameters are case sensitive. You define global parameters in the Parameters node in the model tree under Global Definitions.

4.2.2 Geometry:

This tutorial uses a geometry that was previously created.

The location of the application library that contains the file used in this exercise varies based on the software installation and operating system. In Windows, the file path will be similar to:

C:\Program Files\COMSOL\COMSOL52a\Multiphysics\applications.

1. In the Model Builder window, under Component 1, right-click Geometry 1 and select Import .As an alternative, you can use the ribbon and click Import from the Geometry tab.

2. In the Settings window for Import, from the Source list, select COMSOL Multiphysics file.

3. Click Browse and locate the file wrench. Mph in in the application library folder of the COMSOL installation folder. Its default location in Windows is:

C:\ProgramFiles\COMSOL\COMSOL52a\Multiphysics\applications\COMSOL_Multiphysics\ Structural_Mechanics\wrench.mphbin

Double-click to add or click Open.

4.2.3 Materials

The Materials node stores the material properties for all physics and all domains in a Component node. Use the same generic steel material for both the bolt and tool. Here is how to choose it in the Model Builder.

1. Open the Add Materials window. You can open the Add Materials window in either of these two ways:

-Right-click Component 1 > Materials in the Model Builder and select Add Material

- From the ribbon, select the Home tab and then click Add Material.

2. In the Add Material window, click to expand the Built-In folder. Scroll down to find Structural steel, right-click, and select Add to Component 1.

3. Examine the Material Contents section in the Settings window for Material to see the properties that are available. Properties with green check marks are used by the physics in the simulation.

4. Close the Add Material window.

4.3 Selecting Boundaries and Other Geometric Entities

When a boundary is unselected, its color is typically gray, the exception being when you use the material Appearance setting available in Materials; To select a boundary, first hover over it. This highlights the boundary in red, assuming the boundary was previously unselected. Now, click to select the boundary by using the left mouse button.

The boundary now turns blue. Its boundary number will appear in the Selection list in the Settings window of the corresponding boundary condition. Once a boundary is selected and you hover over it again, the boundary turns green. If you click a boundary highlighted in green, the boundary is deselected and now turns gray again. The same technique for selecting and deselecting is applicable to geometry objects, domains, boundaries, edges, and points.

4.3.1 Mesh

The mesh settings determine the resolution of the finite element mesh used to discretize the model. The finite element method divides the model into small elements of geometrically simple shapes, in this case tetrahedrons. In each

tetrahedron, a set of polynomial functions is used to approximate the structural displacement field — how much the object deforms in each of the three coordinate directions. In this example, because the geometry contains small edges and faces, you will define a slightly finer mesh than the default setting suggests. This will better resolve the variations of the stress field and give a more accurate result. Refining the mesh size to improve computational accuracy always involves some sacrifice in speed and typically requires increased memory usage.

4.3.2 Study

In the beginning of setting up the model, you selected a Stationary study, which implies that a stationary solver will be used. For this to be applicable, the assumption is that the load, deformation, and stress do not vary in time. To start the solver:

- Right-click Study 1 and select Compute (or press F8).After a few seconds of computation time, the default plot is displayed in the Graphics window. You can find other useful information about the computation in the Messages and Log windows; Click the Messages and Log tabs under the Graphics window to see the kind of information available to you. The Messages window can also be opened from the Windows drop-down list in the Home tab of the ribbon.

4.3.3 Results:

The von Mises stress is displayed in the Graphics window in a default Surface plot with the displacement visualized using a Deformation sub node. Change the default unit (N/m2) to the more suitable MPa as shown in the following steps.

CHAPTER 5

PREVIOUS WORKS

5.1 Introduction

Various porous core PCFs with noticeable material loss properties were reported over the ages. A microstructure core honeycomb band-gap fiber for THz wave guidance was reported by Nielsen et al. but in this case periodicity still needs to be maintained strictly in narrowband fibers to satisfy the Bragg conditions.

A porous core fiber with TOPAS as background material using hexagonal structure in both core and cladding was reported by Uthman et al. reported which showed Effective Material Loss (EML) of 0.12 cm-1 but they didn't mention some important properties for THz applications like dispersion and fraction of power.

A porous core fiber having both flattened dispersion and 80% light confinement within the core area was proposed by Liang et al. Because of having higher absorption loss of 0.432 dB/cm at 1.0 THz, this design has not been so seductive for THz guidance.

Kaijage et al. reported a porous core fiber which warrants effective material loss of 0.076 cm-1 but they did not take into consideration some crucial design issues for THz guidance such as dispersion and core power fraction.

A fiber with hexagonal core and rotate hexagonal cladding was proposed by Islam et al. which showed the EML= 0.066 cm-1 and core power fraction of 0.40. A fiber with octagonal core and cladding structure was proposed by Rana et al. but it showed a material loss of 0.058 cm-1 and they neglect to investigate the dispersion properties of that fiber.

A fiber with octagonal structure in the cladding and circular structure in the core was proposed by Hasan et al. which showed an effective material loss of 0.056 cm-1 but they didn't even mention the single mode condition which is one of the main properties for analyzing a fiber.

A rotated hexagonal core surrounded by a circular shape cladding was reported by Saiful et al. which gave loss of .053 cm-1 but can be further reduced & thus improve the efficiency.

5.2 Overview of Some Important Background Works

- A polarization maintaining ultra-low effective material loss based on slotted core kagome lattice fiber is proposed for terahertz (THz) wave propagation was proposed by Md. Rabiul hasan, Numerical study demonstrates that by using rectangular slotted air holes in the core of the kagome lattice exhibits simultaneously an ultra-high birefringence of 8.22 × 10−2, an ultra-low effective material loss of 0.05 cm−1, and a very low confinement loss of 4.13×10−5 cm−1 at the frequency of 1 THz. Further investigation shows that about half of the total mode power confines into the air slots at 50% core porosity.

- A novel porous-core octagonal photonic crystal fiber (POPCF) for practical low-loss terahertz (THz) wave guiding was suggested by Kaijagge. The POPCF with a porous core surrounded by an air-hole cladding shows a low material absorption loss of ∼0.07 cm−1, or one third of that for the bulk material absorption loss at the operating frequency ∼1 THz. In addition, the confinement loss, bending loss, and effective modal area properties of the

POPCF are also reported and demonstrated to be relatively low. The proposed POPCF has potential applications for efficient transmission of broadband THz radiation.

- A photonic crystal fiber having ultralow material loss and near-zero dispersion at the telecom window which is suitable for THz wave guidance was proposed by Imran Hasan. The numerical results show that ultra-low material absorption loss of 0.056 cm−1 at 1.0 THz and nearly zero flattened dispersion of ±0.18 ps/THz/cm can be obtained from the proposed fiber in the wavelength range of 1.0–1.8 THz.

- This letter reports a photonic crystal fiber having ultralow material loss and near-zero dispersion at the telecom window which is suitable for THz wave guidance. The numerical results show that ultra-low material absorption loss of 0.056 cm−1 at 1.0 THz and nearly zero flattened dispersion of ±0.18 ps/THz/cm can be obtained from the proposed fiber in the wavelength range of 1.0–1.8 THz.

- A new type of dielectric 1Hz waveguide, which evolved from a recent approach from the field of integrated optics, is presented with theoretical and experimental results. Due to the continuity of electric flux density at a dielectric interface, the THz wave is predominantly confined in the virtually lossless low index air core of a high-index dielectric waveguide. Attenuation, dispersion, field enhancement and field confinement properties of the waveguide are discussed and compared to those of other THz waveguide approaches.

5.3 The Design We Followed

Terahertz Sensing in a Hollow Core Photonic Crystal Fiber.

5.3.1 Overview

A hollow core photonic crystal fiber is designed and analyzed for chemical analyte detection in the terahertz frequency range. Using Zeonex as the substrate and at optimal design conditions, simulation results shows a high relative sensitivity of 96.69%, 96.97%, and 97.2% for water, ethanol and benzene respectively. In addition, the sensor shows low EML and negligible confinement loss that is useful for efficient sensing.

Moreover, the obtained high birefringence property is suitable to increase the sensing performance. Using the existing fabrication methods the proposed PCF is feasible to fabricate. Therefore, with such remarkable sensing properties and design flexibility the proposed sensor will open a new window for next generation terahertz research and can potentially be applicable in different food and biomedical industries

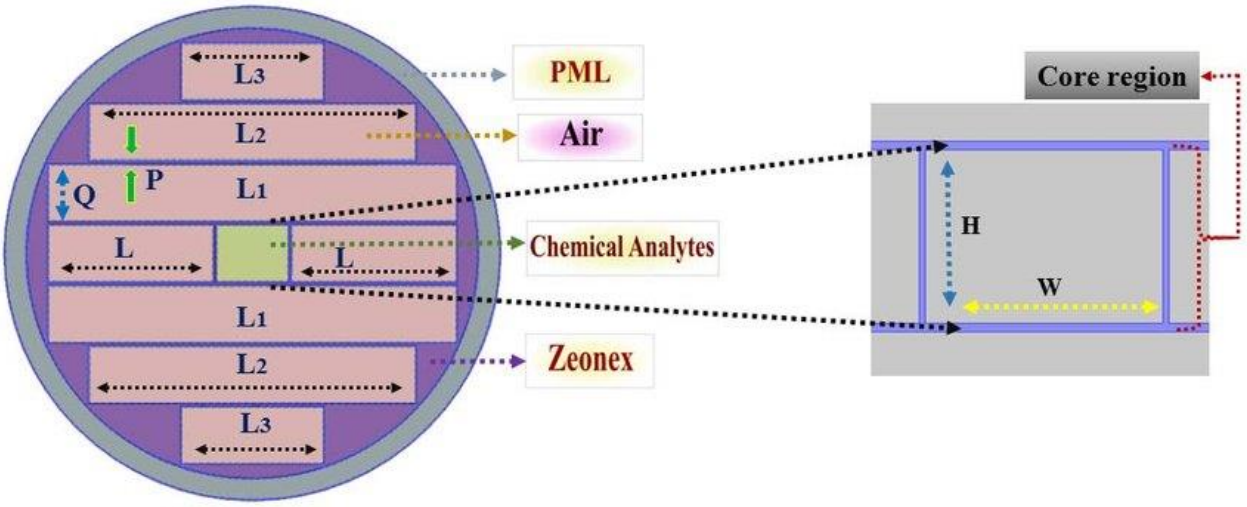

Fig. 1. Cross section of the proposed terahertz sensor.

The cross section of the designed hollow-core (HC) PCF terahertz sensor is shown in Fig. 1. Hollow core fibers are advantageous for sensing applications as the sample under test located in the core can interact with incoming light simultaneously. A hollow core provides lower effective material loss (EML) as well as a higher core power fraction than porous core as the core in a HC-PCF is only filled with the target analyte instead of bulk material. Note that it is a challenging task to maintain the polarization state of a PCF, as sensing performance depends on a highly polarized fiber. High birefringence (i.e. index difference between the polarization modes) can be obtained from the asymmetrical PCF structure that has not been achieved by previously reported sensors. Here, the proposed rectangular hollow core is surrounded by asymmetrical rectangular cladding that provides increased birefringence with improved sensing performance.

In order to design the sensor, full vector finite element method (FEM) based commercially available software COMSOL Multiphysics v5.3 was utilized. The

cladding region is made with a number of rectangular air holes of lengths L, $L1$, $L2$, $L3$. The lengths are maximized at 1105 μm, 2720 μm, 2176 μm, and 952 μm respectively. We defined the air holes width in the cladding as Q and optimized it at 385 μm.We called the defined lengths and width as optimized because we varied those further and found no significant changes in relative sensitivity as varying cladding air holes does not change the amount of analyte filled in the core however may have effect on confinement loss. However, the effect of changes in length of cladding air holes on the sensing performance of the proposed sensor in investigated in later section of the manuscript. Considering the fabrication effectiveness we kept sufficient distance between the air holes that is defined as P. The core region consists of a single asymmetrical air hole that defined it as hollow core. The width and height of the hollow core structure is defined as W and H respectively. A perfectly matched layer (PML) absorbing boundary is given at the outer part of the cladding. The PML boundary condition itself act as an anti-reflecting layer that absorbs outgoing waves of the PCF. It is worthwhile to mention that instead of using air in the hollow core region we uses different chemical analytes such as water, ethanol and benzene with refractive Index (RI) of 1.33, 1.354 and 1.366 respectively. There are a number of polymer materials such as PMMA (Polymethayl-methacrylate), Teflon (Tetrafluroethylyne), Topas (COC), Silica and Zeonex (COP) That can used as a bulk material to design a sensor.We choose Zeonex because of its number of useful optical properties such as constant index of refraction of 1.53

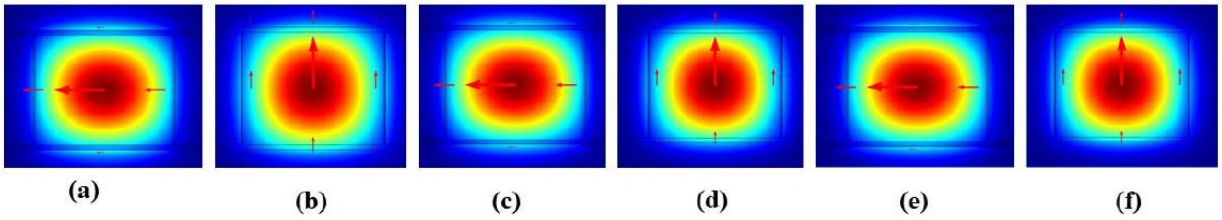

Fig. 2. Mode power distribution of the proposed PC-PCF for: (a) water, X-pol; (b) water, y-pol; (c) ethanol, x-pol; (d) ethanol, y-pol; (e) benzene, X-pol; and (f) benzene, y-pol.

In terahertz range, low absorption loss of 0.2 cm−1, high glass transition temperature *Tg*, negligible water absorption, high biocompatibility and excellent chemical resistance even at elevated temperatures. Note that, Zeonex and Topas have similar optical characteristics but Zeonex has high chemical resistivity and higher bio-compatibility than Topas. Moreover, Zeonex (Grade E-48R) has a higher glass transition temperature than Topas (Grade 5013L-10) that is more suitable for fabrication. Additionally, in some grades of Zeonex such as 330R, 480R and 480 the refractive index is less than Topas and this helps to reduce the effective material loss as refractive index of the background material is directly related to EML (refer to Eqn. 5).

In a PCF based sensor light can be guided either by photonic bandgap (PBG) or by the modified total internal reflection (MTIR) effect. The photonic bandgap mode in a PCF operates when the RI of the cladding is greater than that of the core. On the other hand, the MTIR effect comes into operation when the core RI is greater than that of cladding. In the proposed sensor we used analytes with a high RI, thus

the light guiding mechanism of our proposed sensor is the MTIR mode.

5.3.2 Simulation Results and Discussion

The intensity of light interaction with matter (water, ethanol and benzene) is shown in Fig. 2. It can be seen that for both the polarization mode the light is well guided inside the core. The chemical sensitivity of a terahertz PCF is totally dependent on the intensity of light-matter interaction. This rely on the absorption coefficient at a particular frequency. According to the Beer-Lambert law it can be defined as

$$I(f) = I_0(f)\exp[-r\alpha_m I_c] \quad (1)$$

Where, *I (f)* represent the intensity of light with the presence of analyte need to be sensed and *I*0*(f)* is the intensity without the presence of analyte. Here, *r* , *_m*, *lc,* and *f* represent the relative sensitivity, absorption coefficient, channel Length and the operating frequency respectively. The absorbance of the chemicals to be sensed can be found by

$$A = log\left(\frac{I}{I_0}\right) = -r\alpha_m I_c \quad (2)$$

Now, to investigate the sensing performance of the designed PCF it is necessary to calculate the relate sensitivity that can be calculated by

$$r = \frac{n\pi}{n_{eff}} \times X \quad (3)$$

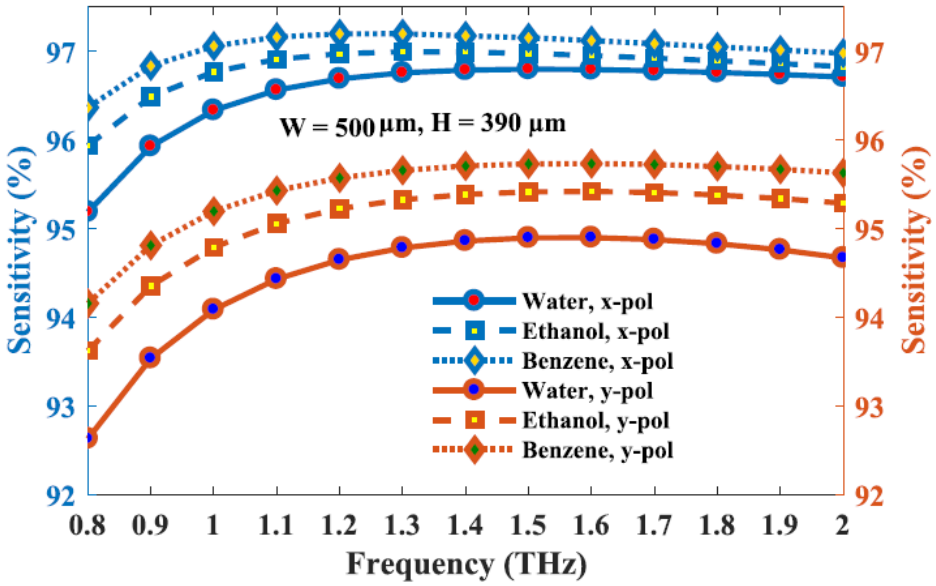

Fig. 3. Relative sensitivity of water, ethanol and benzene as a function of frequency with W = 503 µm and H = 393 µm.

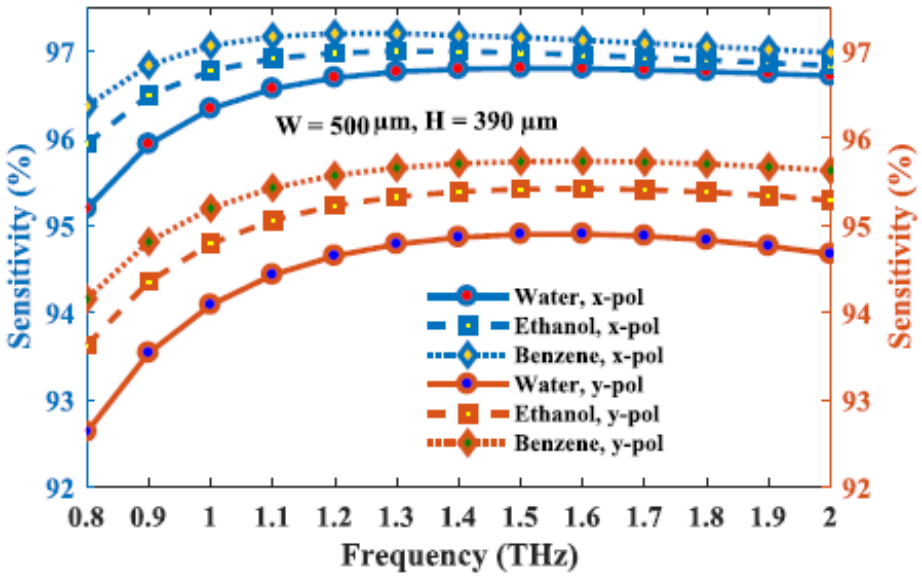

Fig. 4. Relative sensitivity of water, ethanol and benzene as a function of frequency with W = 500 µm and H = 390 µm

Where, *n*r represents the real part of RI of the analyte targeted to be sensed and n_{eff} represents the effective RI of the guided mode respectively. Moreover, *X* represents the amount of light interaction with matter that can be calculated by,

$$X = \frac{\int_{sample} R_e(E_x H_y - E_y H_x) dydx}{\int_{total} R_e(E_x H_y - E_y H_x) dydx} \times 100 \quad (4)$$

Here, E_x, E_y and H_x , H_y are the electric field and magnetic field components of the guided modes respectively. Fig. 3, Fig. 4 and Fig. 5 shows the variation of relative sensitivity of water, ethanol and benzene with respect to frequency. It can be seen that relative sensitivity increases up to a certain frequency and then decreases slightly. This is because, as frequency increases, the effective RI of the guided mode increases but the core power fraction does not increases after a particular frequency. As from Eqn. 3 we can see that the relative sensitivity is proportional to the RI of the analyte and the core power fraction thus relative sensitivity increases with the increase of core power fraction. Moreover, from Eqn. 3 it can also be seen that the relative sensitivity is inversely proportional to the effective RI of the guided mode and thus increase of effective RI reduces the relative sensitivity. Fig. 3, Fig. 4 and Fig. 5 also shows the characteristics variation of relative sensitivity for both the *x* and *y* polarization mode with respect to frequency. It can be seen that the

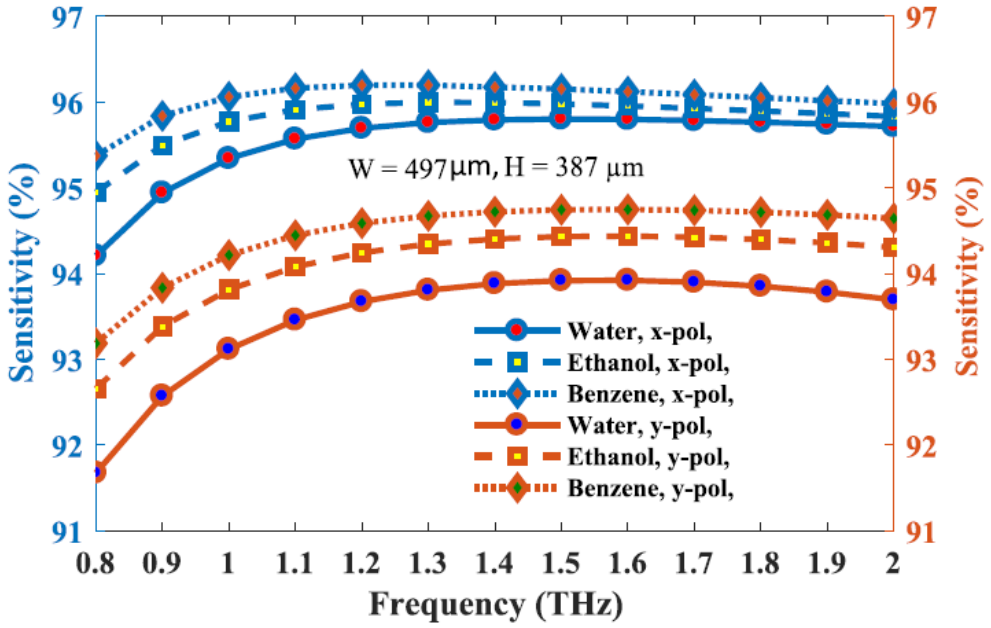

Fig. 5. Relative sensitivity of water, ethanol and benzene as a function of frequency with W = 497 μm and H = 387 μm.

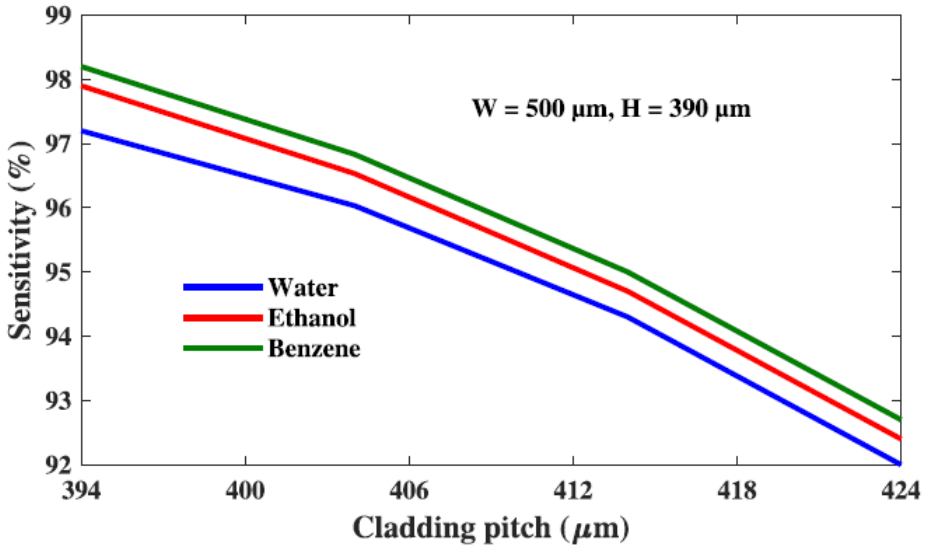

Fig. 6. Relative sensitivity of water, ethanol and benzene as a function of cladding pitch variation with W = 500 μm and H = 390 μm.

Obtained relative sensitivity for *x* polarization mode is higher than the obtained relative sensitivity for the *y* polarization mode. This is because the proposed PCF is birefringent thus we get different characteristics in different polarization modes. We obtain higher relative sensitivity in *x* polarization mode because in that mode the obtained core power fraction is higher than *y* polarization mode. The performance of relative sensitivity with the variation of W and *H* is also investigated that is shown through Fig. 3, Fig. 4 and Fig. 5. It is found that the relative sensitivity increases with the increase of *W* and *H*. It can also be found that maximum relative sensitivity is obtained at $W = 503\ \mu$m and $H = 393\ \mu$m. Please note that, $W = 503\ \mu$m and $H = 393\ \mu$m is the maximum width and height of the core and further increment may overlap the core with the cladding. To further investigate the sensing performance we varied *W* and *H* and found that relative sensitivity decreases when we decreases *W* and *H*. Thus, keeping sufficient distance between the core and cladding for flexible fabrication we choose $W = 500\ \mu$m and $H = 390\ \mu$m as optimum. Next, changing the cladding pitch (center to center distance between cladding air holes) we observed the sensing performance Of the sensor that is shown in Fig. 6. We can see that as the pitch increases the relative sensitivity goes down because that also reduces the core power fraction. In order to optimize the length of cladding air holes we varied the lengths and calculated the relative sensitivity of water as an example. Fig. 7 shows the variation of refractive

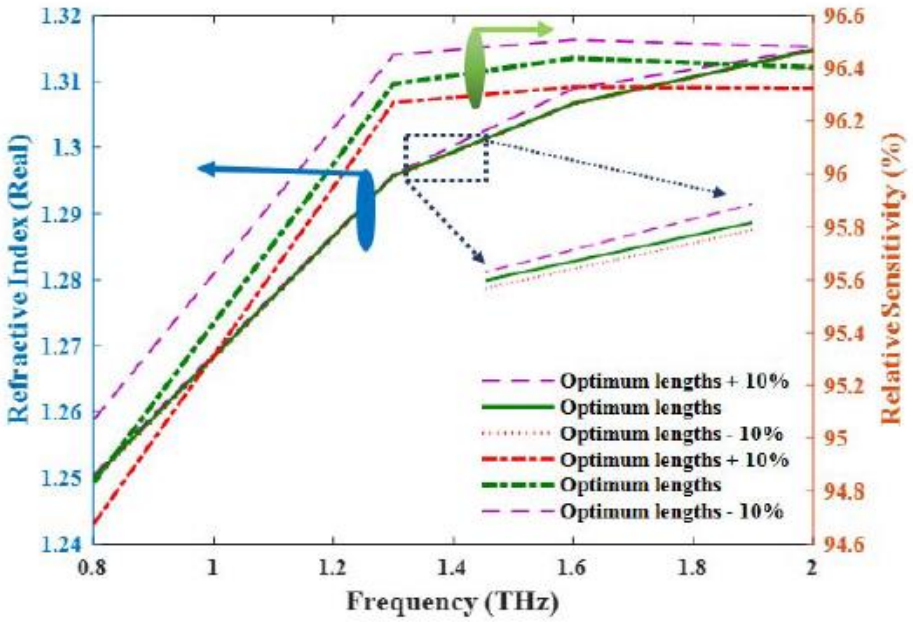

Fig. 7. Relative sensitivity of water with the variation of cladding air holes lengths as a function of frequency with W = 500 µm and H = 390 µm and Q = 394 µm.

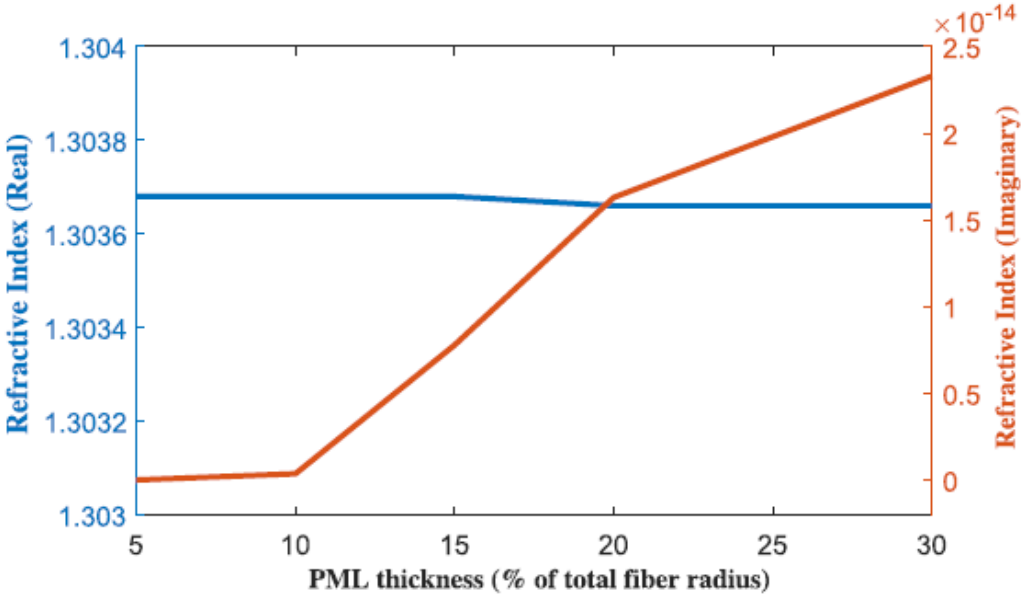

Fig. 8. Variation of refractive index with respect to PML variation at W = 500 µm, H = 390 µm, Q = 394 µm and f = 1.4 THz.

Index (real) and relative sensitivity for water with variation of cladding air holes lengths with respect to frequency. It can be seen that changing the cladding air hole lengths has very little impact on the sensing performance of the PCF. However, longer air hole lengths increases the cladding size, allowing strong confinement of optical signals as a result of reduced confinement loss. However, this also increases the size of the sensor and makes it bulky. Therefore, considering the size and fabrication tolerance of the PCF we choose the optimum lengths as described in Section II. It is also important to optimize the PML thickness. Keeping all other parameters optimum we did the convergent test to choose the PML thickness that is shown in Fig. 8. It can be seen from Fig. 8 that the variation of real part of RI with respect to PML thickness is negligible. As relative sensitivity is dependent on the real part of RI thus change of PML thickness does not affect the variation of relative sensitivity. However, the imaginary part of complex RI changes with PML thickness variation that affects the confinement loss as confinement loss is dependent on the imaginary part of the complex RI. However, the effect of change (Imaginary part of RI) is minimum as the RI of the core is very high (1.33/1.354/1.366) than that of cladding RI (1.0). Thus strong MTIR effect works there to confine the light strongly in the core region. We can see that the complex imaginary part is

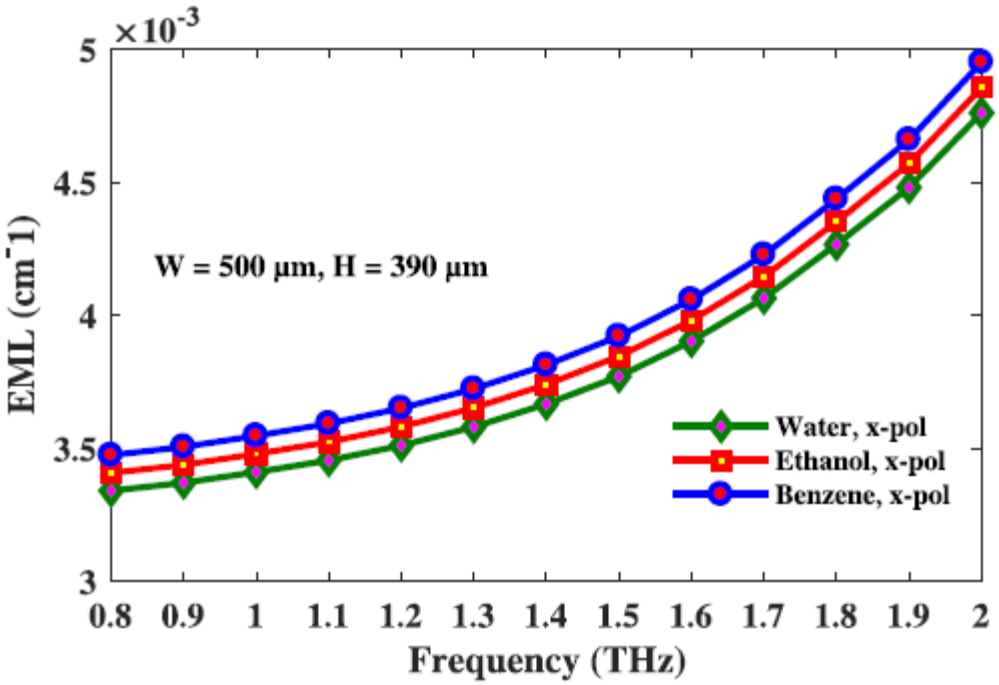

Fig. 9. Effective material loss of water, ethanol and benzene as a function of frequency at W = 500 μm and H = 390 μm, Q = 394 μm.

higher at 5% of the total fiber radius but considering the fabrication effectiveness we choose the optimal PML thickness as 10% of the total fiber radius.

Therefore, observing the characteristics of relative sensitivity from Fig. 3, Fig. 4, Fig. 5, 6, and 7 of water, ethanol and benzene with different parameter variation it can be seen that they have very similar response with respect to frequency.
In practice, fluids such as water, ethanol and benzene can be distinguished due different absorption coefficients as a function of frequency.

In a terahertz sensor there are few limiting factors such as effective material loss (EML), confinement loss, bending loss and scattering loss that limits the efficient detection of analytes. Please note that, we neglect to investigate the scattering loss

property as from Fig. 2 it is clearly observed that the light is well confined in the core and interaction of light with the cladding is negligible. Moreover, considering the length of the sensor we also neglect to characterize the bending loss of the PCF. Among these the major loss mechanism is EML that occurs due to the used background material and can be reduced by using air holes inside the core region. Another reason of choosing hollow core is that, it can largely reduce the amount of background material from the core and thus helps to reduce the EML. The EML of a PCF can be calculated by the equation

$$\alpha_{eff} = \sqrt{\frac{\varepsilon}{\mu}}\left(\frac{\int_{mat} n_{mat}|E|^2 \alpha_{mat} dA}{|\int_{all} S_z dA|}\right) \quad (5)$$

Where, ε and μ designates the permittivity and permeability in free space, _mat and n_{mat} indicates the bulk material loss and the RI of Zeonex and S_z implies the *z*-component of Poynting vector S_z= 12*(***E** × **H***) z*, here, **E** is the electric Field component and **H**_ is the magnetic field component. The characteristics of EML with respect to frequency with different analyte variation is shown in Fig. 9. It can be seen that EML increases with frequency increase that meets the theoretical condition of calculating EML. It can be seen from Fig. 9 that the EML at optimum design conditions is extremely low and lowest than ever proposed by any PCF based waveguide. Another limiting factor that specifies the length of terahertz sensor is confinement loss. Confinement loss depends on the

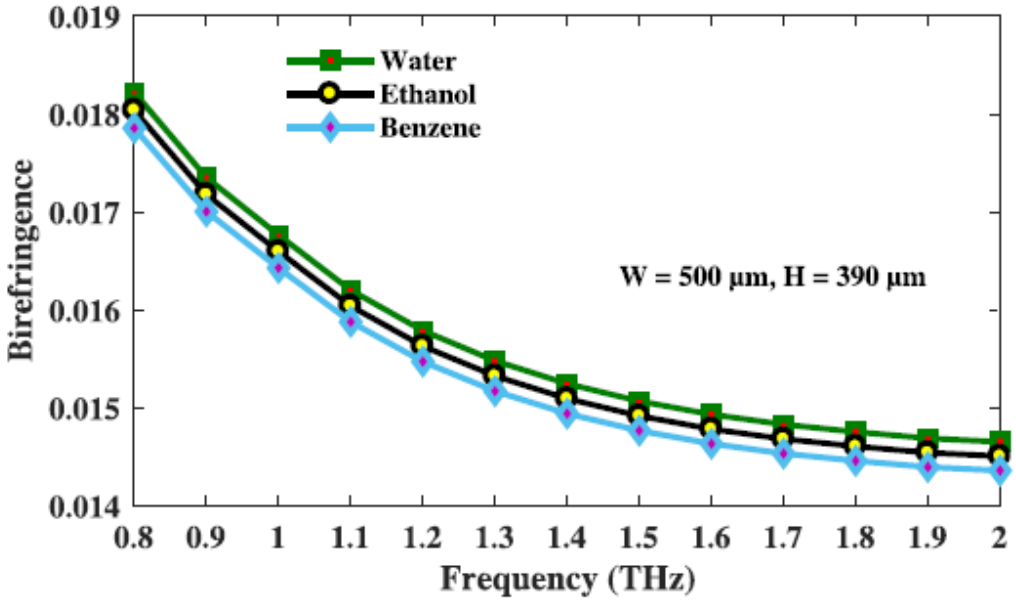

Fig. 10. Confinement loss of water, ethanol and benzene as a function of Frequency at W = 500 µm and H = 390 µm, Q = 394 µm.

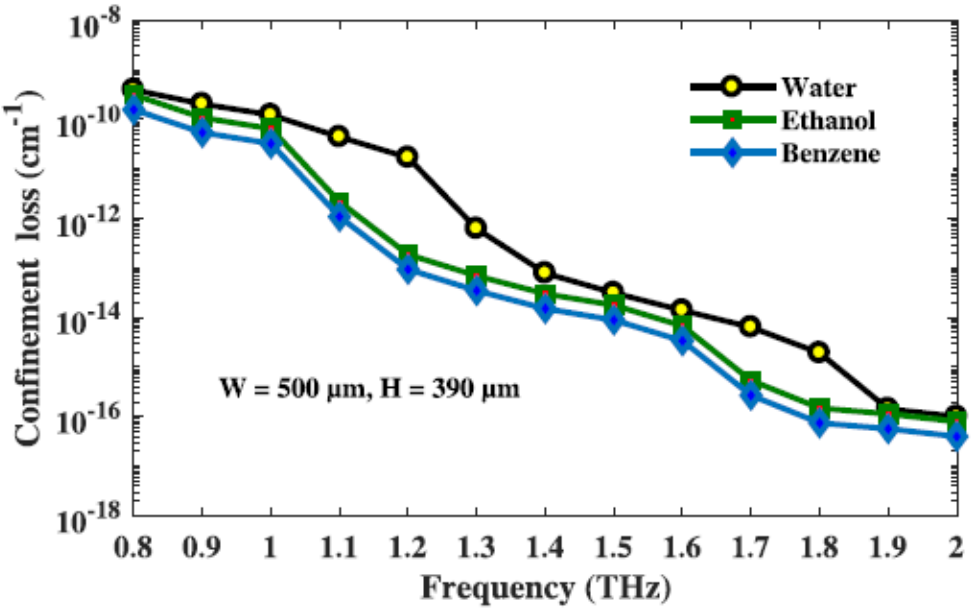

Fig. 11. Birefringence of water, ethanol and benzene as a function of frequency at W = 500 µm and H = 390 µm, Q = 394 µm.

Imaginary part of complex RI of the guided mode. It can be characterized by the following equation [13],

$$L_c = \left(\frac{4\pi f}{c}\right) \mathrm{Im}\left(n_{eff}\right) \tag{6}$$

Here, $\mathrm{Im}\left(n_{eff}\right)$ indicates the imaginary part of the effective RI. Fig. 10 indicates the variation of confinement loss for different analytes with respect to frequency. It is observed that confinement loss reduces with frequency increase because increment of frequency causes the mode fields to constrict more strictly in the hollow core region and thus the confinement loss reduces. It can be seen that the obtained confinement loss for water ($6.22\times 10{-}13 cm^{-1}$), ethanol ($6.95\times 10{-}14 cm^{-1}$) And benzene ($3.48 \times 10{-}14\ cm^{-1}$) is negligible as compared to the obtained EML.The polarization maintaining property of a fiber is important in improving the sensing performance of a sensor. Birefringence is the property that measures polarization state of a PCF. It can be calculated by the following equation [6],

$$B = |n_x - n_y| \tag{7}$$

Here, n_x and n_y represents the mode index in the *x* and *y*-polarization mode respectively. The property of birefringence for different analyte variation is shown in Fig. 11. It can be seen that birefringence reduces with frequency increase. The reason is that, as the frequency increases the index difference between the polarization modes also decreases. At optimum design parameters the obtained birefringence for water, ethanol and benzene are 0.15, 0.17, and 0.19 respectively. Please note that, it is potentially possible to increase the birefringence further by reducing either *W* or *H* but that will significantly reduce the relative sensitivity.

5.3.3 Sensor Architecture and Sensing Mechanism

The obtained relative sensitivity of water, ethanol and benzene for different *W* and *H* is compared in Table I. It can be seen from Table I that, highest relative sensitivity is obtained for benzene with maximum *W* and *H*. The reason is that, at maximum *W* and *H* the hollow core can load maximum

TABLE I
COMPARISON OF SENSING PERFORMANCE WITH GLOBAL PARAMETER VARIATION OF THE PCF

W and H	Operating frequency	Sensitivity of water (%)	Sensitivity of ethanol (%)	Sensitivity of Benzene (%)
497 μm and 387 μm	1.5 THz	95.6	95.9	96.2
500 μm and 390 μm	1.5 THz	96.4	96.6	97.2
503 μm and 393 μm	1.5 THz	97.6	97.9	98.2

TABLE II
COMPARISON OF CHARACTERISTICS BETWEEN THE PROPOSED SENSOR AND PRIOR SENSOR FOR CHEMICAL (ETHANOL FOR EXAMPLE) ANALYTE DETECTION

Ref.	Operating Region	Relative Sensitivity (%)	EML (cm^{-1})	Confinement loss (cm^{-1})	Birefringence
[12]	1.5 μm	23.75	-	5.5×10^{-5}	-
[44]	1.33 μm	67.66	-	7.5×10^{-12}	-
[25]	1.6 THz	85.7	-	1.7×10^{-9}	0.005
This manuscript	1.4 THz	96.8	0.0035	6.95×10^{-14}	0.0154

amount of analyte into it. Another reason for obtaining highest sensitivity with benzene is its higher RI compared to other used analytes. Considering ethanol as the chemical analyte, Table II shows the comparison of different characteristics of the proposed PCF and prior PCF. It can be observed that, the proposed PCF has the highest sensitivity because of the hollow core that can load more analyte than porous core described in. Moreover, besides high birefringence the proposed PCF based terahertz sensor also demonstrate extremely low EML and negligible confinement loss than obtained by prior PCFs.

CHAPTER 6

BACKGROUND MATERIAL

Background Material: Zeonex

6.1 Glass-Like Optical Properties

ZEONEX Cyclo Olefin Polymer (COP) optical polymers exhibit glass-like transparency from UVA through NIR wavelengths. With a refractive index of 1.53 and ABBE number of 56, ZEONEX Cyclo Olefin Polymer (COP) combines the optical characteristics of glass with the design freedom of a molded plastic.

6.2 Low Birefringence

ZEONEX Cyclo Olefin Polymer (COP) achieves very low total birefringence by combining low intrinsic birefringence with an ultra-low photoelastic constant for excellent stress birefringence performance. Compared with other polymers, the higher molding temperature capability of Cyclo Olefin Polymer (COP) also promotes improved birefringence by allowing for reduced molecular orientation during molding.

6.3 Low Moisture and High Temperature Stability

ZEONEX Cyclo Olefin Polymer (COP) has <0.01% water absorption – significantly less than polycarbonate (PC) and acrylic polymethyl methacrylate (PMMA). Lenses made with ZEONEX Cyclo Olefin Polymer (COP) are dimensionally stable, and show minimal change of optical properties following exposure to varying humidity environments.

6.4 Blue and NIR Laser Capability

ZEONEX Cyclo Olefin Polymer (COP) optical grades are engineered to meet requirements of high-performance and specialty applications. Certain grades of ZEONEX Cyclo Olefin Polymer (COP) offer good resistance to long-term exposure to blue light and NIR wavelengths, such as those found in blue laser optical pick-up systems and 3D position sensing.

CHAPTER 7

FACTORS AND LOSSES IN OPTICAL FIBER

7.1 Single Mode Fiber

In fiber-optic communication, a **s**ingle-mode optical fiber (SMF) is an optical fiber designed to carry light only directly down the fiber - the transverse mode. Modes are the possible solutions of the Helmholtz equation for waves, which is obtained by combining Maxwell's equations and the boundary conditions. These modes define the way the wave travels through space, i.e. how the wave is distributed in space. Waves can have the same mode but have different frequencies. This is the case in single-mode fibers, where we can have waves with different frequencies, but of the same mode, which means that they are distributed in space in the same way, and that gives us a single ray of light. Although the ray travels parallel to the length of the fiber, it is often called transverse mode since its electromagnetic vibrations occur perpendicular (transverse) to the length of the fiber. The 2009 Nobel Prize in Physics was awarded to Charles K. Kao for his theoretical work on the single-mode optical fiber.

7.1.1 Characteristics:

Like multi-mode optical fibers, single mode fibers do exhibit modal dispersion resulting from multiple spatial modes but with narrower modal dispersion. Single mode fibers are therefore better at retaining the fidelity of each light pulse over longer distances than multi-mode fibers. For these reasons, single-mode fibers can

have a higher bandwidth than multi-mode fibers. Equipment for single mode fiber is more expensive than equipment for multi-mode optical fiber, but the single mode fiber itself is usually cheaper in bulk.

A typical single mode optical fiber has a core diameter between 8 and 10.5 μm and a cladding diameter of 125 μm. There are a number of special types of single-mode optical fiber which have been chemically or physically altered to give special properties, such as dispersion-shifted fiber and nonzero dispersion-shifted fiber. Data rates are limited by polarization mode dispersion and chromatic dispersion. As of 2005, data rates of up to 10 gigabits per second were possible at distances of over 80 km (50 mi) with commercially available transceivers (Xenpak). By using optical amplifiers and dispersion-compensating devices, state-of-the-art DWDM optical systems can span thousands of kilometers at 10 Gbit/s, and several hundred kilometers at 40 Gbit/s.

The lowest-order bounds mode is ascertained for the wavelength of interest by solving Maxwell's equations for the boundary conditions imposed by the fiber, which are determined by the core diameter and the refractive indices of the core and cladding. The solution of Maxwell's equations for the lowest order bound mode will permit a pair of orthogonally polarized fields in the fiber, and this is the usual case in a communication fiber.

In step-index guides, single-mode operation occurs when the normalized frequency, *V*, is less than or equal to 2.405. In practice, the orthogonal polarizations may not be associated with degenerate modes.

$$V = \frac{2\pi r f}{c}\sqrt{{n_{co}}^2 - {n_{cl}}^2} \leq 2.405$$

OS1 and OS2 are standard single-mode optical fiber used with wavelengths 1310 nm and 1550 nm (size 9/125 μm) with a maximum attenuation of 1 dB/km (OS1) and 0.4 dB/km(OS2). OS1 is defined in ISO/IEC 11801, [7] and OS2 is defined in ISO/IEC 24702.

7.2 Multi Mode Fiber

Multi-mode optical fiber is a type of optical fiber mostly used for communication over short distances, such as within a building or on a campus. Typical multimode links have data rates of 10 Mbit/s to 10 Gbit/s over link lengths of up to 600 meters (2000 feet).

7.2.1 Applications

The equipment used for communications over multi-mode optical fiber is less expensive than that for single-mode optical fiber. Typical transmission speed and distance limits are 100 Mbit/s for distances up to 2 km (100BASE-FX), 1 Gbit/s up to 1000 m, and 10 Gbit/s up to 550 m.

Because of its high capacity and reliability, multi-mode optical fiber generally is used for backbone applications in buildings. An increasing number of users are taking the benefits of fiber closer to the user by running fiber to the desktop or to the zone. Standards-compliant architectures such as Centralized Cabling and fiber to the telecom enclosure offer users the ability to leverage the distance capabilities of fiber by centralizing electronics in telecommunications rooms, rather than having active electronics on each floor.

7.2.2 Comparison with Single-Mode Fiber

The main difference between multi-mode and single-mode optical fiber is that the former has much larger core diameter, typically 50–100 micrometers; much larger than the wavelength of the light carried in it. Because of the large core and also the possibility of large numerical aperture, multi-mode fiber has higher "light-gathering" capacity than single-mode fiber. In practical terms, the larger core size simplifies connections and also allows the use of lower-cost electronics such as light-emitting diodes (LEDs) and vertical-cavity surface-emitting lasers (VCSELs) which operate at the 850 nm and 1300 nm wavelength (single-mode fibers used in telecommunications typically operate at 1310 or 1550 nm). However, compared to single-mode fibers, the multi-mode fiber bandwidth–distance product limit is lower. Because multi-mode fiber has a larger core-size than single-mode fiber, it supports more than one propagation mode; hence it is limited by modal dispersion, while single mode is not.

The LED light sources sometimes used with multi-mode fiber produce a range of wavelengths and these each propagate at different speeds. This chromatic dispersion is another limit to the useful length for multi-mode fiber optic cable. In contrast, the lasers used to drive single-mode fibers produce coherent light of a single wavelength. Due to the modal dispersion, multi-mode fiber has higher pulse spreading rates than single mode fiber, limiting multi-mode fiber’s information transmission capacity.

Single-mode fibers are often used in high-precision scientific research because restricting the light to only one propagation mode allows it to be focused to an intense, diffraction-limited spot.

Jacket color is sometimes used to distinguish multi-mode cables from single-mode ones. The standard TIA-598C recommends, for non-military applications, the use of a yellow jacket for single-mode fiber, and orange or aqua for multi-mode fiber, depending on type. Some vendors use violet to distinguish higher performance OM4 communications fiber from other types.

7.3 Material Absorption Loss

Absorption of signal is a serious loss mechanism in an optical fiber. Absorption occurs in optical fibers due to the presence of imperfections in the atomic structure of the fiber material, due to some basic inherent intrinsic material properties and due to some extrinsic material properties. Imperfections may appear in atomic structure due to oxygen deficiencies and missing of certain molecules. Diffusion of hydrogen molecules may also induce absorption. But the contribution from imperfections is relatively small in fiber optic absorption losses. Inherent intrinsic absorption is caused by basic fiber material properties. If a material is free from impurities and imperfections, then entire absorption is due to intrinsic absorption. Silica fibers possess very low intrinsic material absorption. Here absorption is caused by the vibration of silicon-oxygen bonds. The interaction between these bonds and the electromagnetic field of the optical signal is responsible for intrinsic absorption. Presence of impurities in the fiber material leads to extrinsic absorption. This is caused by the electronic transition of metal impurity ions from one energy level to another. Another reason for extrinsic absorption is the presence of hydroxyl ions in the fiber.

$$\alpha_{eff} = \sqrt{\frac{\varepsilon}{\mu}}\left(\frac{\int_{mat} n_{mat}|E|^2 \alpha_{mat} dA}{\left|\int_{all} S_z dA\right|}\right)$$

Where, $\varepsilon 0$ and $\mu 0$ are considered to be the relative permittivity and permeability in vacuum respectively, n_{mat} is the refractive index of Topas, α_{mat} is the bulk material absorption loss, ***E*** is the modal electric field and S_z is the z component of the pointing vector (S_z= ½(**E** × **H***).z), where **E** and **H** are the electric and magnetic fields respectively.Fig.5 depicts the characteristics of EML as a function of core diameter with different core porosities. From where it is observed that, for the same porosity values there is a significant change of EML when the core diameter changes.

It is a loss mechanism related to the material composition and fabrication process of the fiber which results in the dissipation of some of the transmitted optical power as heat in waveguide. The absorption of light may be intrinsic (caused by one or more major components of glass) or extrinsic (caused by impurities within the glass).

7.4 Mode Power Propagation

The amount of useful power propagating through different regions of the fiber also known as core power fraction can be calculated by,

$$\eta' = \frac{\int_x S_z dA}{\int_{all} S_z dA}$$

Where η′ represents mode power fraction and X represents the area of interests. To design a standard PCF, it is necessary to pass most of the useful power through the core air holes. Higher Dcore increases the core power fraction but this also increases the EML. On the other hand, as the Dcore decreases EML also decreases but this

also decreases the core power fraction. These are contradictory conditions and needs to select an optimum condition of higher core power fraction and lower EML. At different core porosities, the characteristics of core power fraction as a function of core diameter where it can be observed that amount of core power increases with the increase of core diameter.

7.5 Confinement Loss

PCFs are a new class of optical fibers, which has concerned fabulous attention in the last few years. PCFs are normally formed with silica having air holes positioned in the cladding region. PCFs have novel properties because the effective refractive index has burly wavelength dependence and huge design flexibility. PCFs main applications range from telecommunication field to metrology, spectroscopy, microscopy, medical diagnostics equipment, biology and sensing. There are several parameters to manipulate: pitch, air hole shape and diameter, refractive index of the glass, and type of lattice. PCFs structures can have hexagonal lattice or octagonal lattice or square lattice. By changing the lattices and lattice parameters like pitch, air hole diameter and changing rings in the cladding region, the properties of PCFs can also be changed.

Many experiments and investigations have been carried out using different analysis techniques and tools to understand the propagation properties of various PCFs. PCFs also known as micro-structured or holey fibers are made of the refractive index periodicity, with the arrangement of air holes around the core. Many rings around the core help to ensnare light well within the core minimizing the confinement loss. Based on structure, PCFs can be either solid core high-index guiding fibers or hollow core low index guiding fibers. The index guiding PCFs guide light in a solid core by

modified total internal reflection (M-TIR) like to the conventional optical fibers. Hollow core PCFs guide light by the photonic band gap (PBG) effect. Light is confined in the low-index core, as the distribution of energy levels in the structure makes the propagation in the cladding region impossible. In both cases, to attain the lowest amount loss, air holes should be continual to infinity which is unfeasible. So, modes leak in cladding and confinement loss is created. The confinement loss can be reduced by proper design of structure parameters in PCFs, and consequently, mode leakage to cladding is avoided. Already, many reports have been published about PCFs with low confinement loss. At 0.8 μm center wavelength the confinement loss is found 10-8dB/m, 10-6dB/m and 10-4 dB/m for 2 μm, 1.8 μm and 1.6 μm lattice pitches. Again at 1.55 μm center wavelength for

three rings hexagonal PCFs the confinement loss is 10-3 dB/km but Ademgil and Huxha obtained this loss which was varied from 10-1to 10-5dB/m [10]. Also at 1.3 μm center wavelength this confinement loss was found 10-8dB/km for circular ring PCFs.

Another important parameter to be considered for PCF design is confinement loss. It depends upon the core porosity and the number of air holes used in cladding. It can be calculated by taking the imaginary part of the complex refractive index. The confinement loss can be calculated by,

$$L_c = 8.686 \left(\frac{2\pi f}{c}\right) \mathrm{Im}(n_{eff}) \left(\frac{dB}{m}\right)$$

Where, f is the frequency of the guiding light, c is speed of light in vacuum and $\mathrm{Im}(n_{eff}))$ symbolizes the imaginary part of the refractive index. The confinement loss as a function of frequency where it is observed that as the frequency increases, the confinement loss scaled down.

7.6 Dispersion

In optics, dispersion is the phenomenon in which the phase velocity of a wave depends on its frequency. Media having this common property may be termed dispersive media. Sometimes the term chromatic dispersion is used for specificity. Although the term is used in the field of optics to describe light and other electromagnetic waves, dispersion in the same sense can apply to any sort of wave motion such as acoustic dispersion in the case of sound and seismic waves, in gravity waves (ocean waves), and for telecommunication signals propagating along transmission lines (such as coaxial cable) or optical fiber.

In optics, one important and familiar consequence of dispersion is the change in the angle of refraction of different colors of light, as seen in the spectrum produced by a dispersive prism and in chromatic aberration of lenses. Design of compound achromatic lenses, in which chromatic aberration is largely cancelled, uses a quantification of a glass's dispersion given by its Abbe number V, where lower Abbe numbers correspond to greater dispersion over the visible spectrum. In some applications such as telecommunications, the absolute phase of a wave is often not important but only the propagation of wave packets or "pulses"; in that case one is interested only in variations of group velocity with frequency, so-called group-velocity dispersion (GVD).

7.6.1 Material and Waveguide Dispersion

Most often, chromatic dispersion refers to bulk material dispersion, that is, the change in refractive index with optical frequency. However, in a waveguide there is also the phenomenon of waveguide dispersion, in which case a wave's phase velocity

in a structure depends on its frequency simply due to the structure's geometry. More generally, "waveguide" dispersion can occur for waves propagating through any inhomogeneous structure (e.g., a photonic crystal), whether or not the waves are confined to some region. In a waveguide, both types of dispersion will generally be present, although they are not strictly additive. For example, in fiber optics the material and waveguide dispersion can effectively cancel each other out to produce a Zero-dispersion wavelength, important for fast Fiber-optic communication.

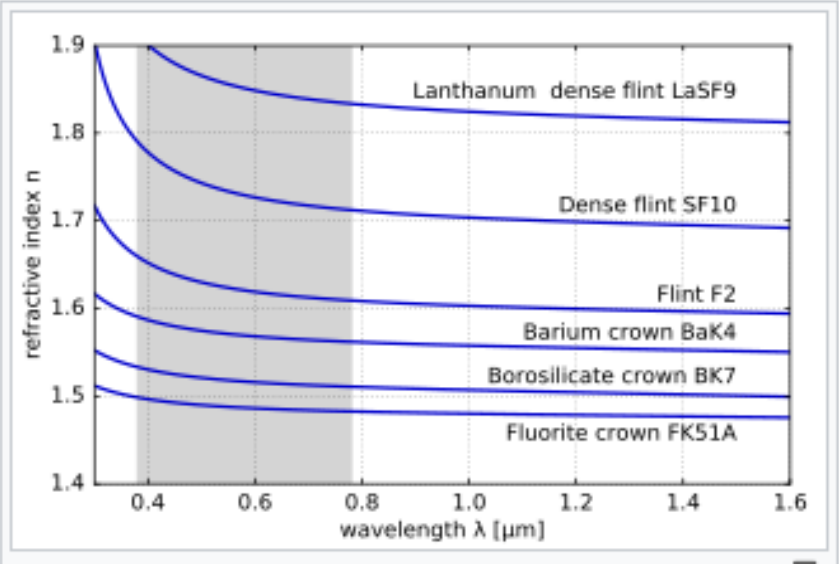

The variation of refractive index vs. vacuum wavelength for various glasses. The wavelengths of visible light are shaded in red.

Influences of selected glass component additions on the mean dispersion of a specific base glass (nF valid for $\lambda = 486$ nm (blue), nC valid for $\lambda = 656$ nm (red).

Material dispersion can be a desirable or undesirable effect in optical applications. The dispersion of light by glass prisms is used to construct spectrometers and spectro

radiometers. Holographic gratings are also used, as they allow more accurate discrimination of wavelengths. However, in lenses, dispersion causes chromatic aberration, an undesired effect that may degrade images in microscopes, telescopes and photographic objectives.

In general, the refractive index is some function of the frequency f of the light, thus n = n(f), or alternatively, with respect to the wave's wavelength n = n(λ). The wavelength dependence of a material's refractive index is usually quantified by its Abbe number or its coefficients in an empirical formula such as the Cauchy or Sellmeier equations.

Because of the Kramers–Kronig relations, the wavelength dependence of the real part of the refractive index is related to the material absorption, described by the imaginary part of the refractive index (also called the extinction coefficient). In particular, for non-magnetic materials (μ = μ0), the susceptibilityχ that appears in the Kramers–Kronig relations is the electric susceptibility $\chi_e = n^2 - 1$

In this case, the medium is said to have normal dispersion. Whereas, if the index increases with increasing wavelength (which is typically the casefor X-rays, the medium is said to have anomalous dispersion.

At the interface of such a material with air or vacuum (index of ~1), Snell's law predicts that light incident at an angle θ to the normal will be refracted at an angle arc sin(sin θ/n). Thus, blue light, with a higher refractive index, will be bent more strongly than red light, resulting in the well-known rainbow pattern.

7.6.2 Dispersion in Waveguides

Waveguides are highly dispersive due to their geometry (rather than just to their material composition). Optical fibers are a sort of waveguide for optical frequencies (light) widely used in modern telecommunications systems. The rate at which data can be transported on a single fiber is limited by pulse broadening due to chromatic dispersion among other phenomena.

In general, for a waveguide mode with an angular frequencyω (β) at a propagation constantβ (so that the electromagnetic fields in the propagation direction z oscillate proportional to ei(βz−ωt)), the group-velocity dispersion parameter D is defined as:

$$\beta_2 = \frac{2}{c}\frac{dn_{eff}}{d\omega} + \frac{\omega}{c}\frac{d^2 n_{eff}}{d\omega^2}$$

Where λ = 2πc/ω is the vacuum wavelength and vg = dω/dβ is the group velocity. This formula generalizes the one in the previous section for homogeneous media, and includes both waveguide dispersion and material dispersion. The reason for defining the dispersion in this way is that |D| is the (asymptotic) temporal pulse spreading Δt per unit bandwidth Δλ per unit distance travelled, commonly reported in ps / nm km for optical fibers.

In the case of multi-mode optical fibers, so-called modal dispersion will also lead to pulse broadening. Even in single-mode fibers, pulse broadening can occur as a result of polarization mode dispersion (since there are still two polarization modes). These are not examples of chromatic dispersion as they are not dependent on the wavelength or bandwidth of the pulses propagated.

7.7 Effective Area:

The effective area (A_{eff}) of the proposed fiber is also discussed, which can be calculated by [33]

$$A_{eff} = \frac{[\int I(r) r dr]^2}{[\int I^2(r) dr]^2}$$

Where; I(r) = |Et| 2is defined as the transverse electric field intensity distribution in the cross section of the fiber. The A_{eff} as a function of frequency, from where it is observed that as the frequency increases from 0.9 THz the A_{eff} decreases. It is because of more light spread for f>1 THz. It is also observed that at operating parameters, the calculated A_{eff} is very much comparable.

CHAPTER 8

OUR PROPOSED DESIGN

8.1 Overview

A novel hollow core photonic crystal fiber (PCF) is presented which consists of symmetrical hexagonal rings in its cladding distributed in three rows. The prime objective of this work is to increase the sensitivity but other significant features like effective material loss, confinement loss, effective area, numerical aperture and dispersion have been thoroughly investigated over a wide bandwidth using the finite element method-based commercially available software, COMSOL version 5.3. Numerical simulation shows that, a maximum chemical sensitivity of 99.39%, 99.76% and 99.44% can be obtained for methanol, benzene and water respectively at optimum operating conditions. The symmetry in design makes the proposed structure easily feasible to be fabricated using the existing fabrication technologies. Thus it is believed that the proposed PCF has the potential to uplift the standard of photonic crystal fiber sensors and open a new window in this field of research.

8.2 Main Design and Methodology

Proposed PCF sensor's cross section is represented by Fig. 1. Three layers of air rings are used to create the cladding which surrounds the hollow core. The air holes are hexagonal by nature and each of the same size. Note that, PCF with similar hexagonal air hole based cladding were also introduced for terahertz transmission application where they also used a number of smaller hexagonal air hole in the core [62]. Assume each hexagonal air hole's center to any vertex distance is n and vertex

to vertex is located by maintaining the distance $2n$. Cladding pitch which is actually center to center distance of two air holes is 180 µm. n is chosen equal to 100 µm for the proposed model in optimum condition. In this condition, distance between two hexagonal air holes of the cladding is 6.8µm and is termed as strut as shown in Fig. 1. Though the standard protocol accepts generally $\pm 2\%$ variation of global parameters of a PCF sensor [33], strut value was varied by $\pm 10\%$ which justifies the acceptance of the global parametric variation. When strut is varied, the n parameter remains constant and as well as the size of the hexagon. When n is varied between 100µm to 96µm, the distance between air holes of the cladding (cladding pitch) remains same by compressing the hexagonal size accordingly. The diameter of the horizontal and vertical axis of the hollow core is $6\sqrt{n^2-\left(\frac{n}{2}\right)^2}$ and $4n$ respectively.

It was realized in previous experiments that the background materials of PCF has strong connection to the sensor characteristics. The sensing response, confinement loss, effective area and numerical aperture are affected simultaneously due to material background [34]. Teflon, Topas, Silica, Zeonex etc. can be used as background material [35-37]. Zeonex E48R (Sultan ova) has been used for the proposed sensor as it has extremely low water absorption rate (less than 0.01% per 24 hours) which enables properties like excellent dimensional stability even under high humidity conditions and high transparency (92% in visible range 400-800nm).

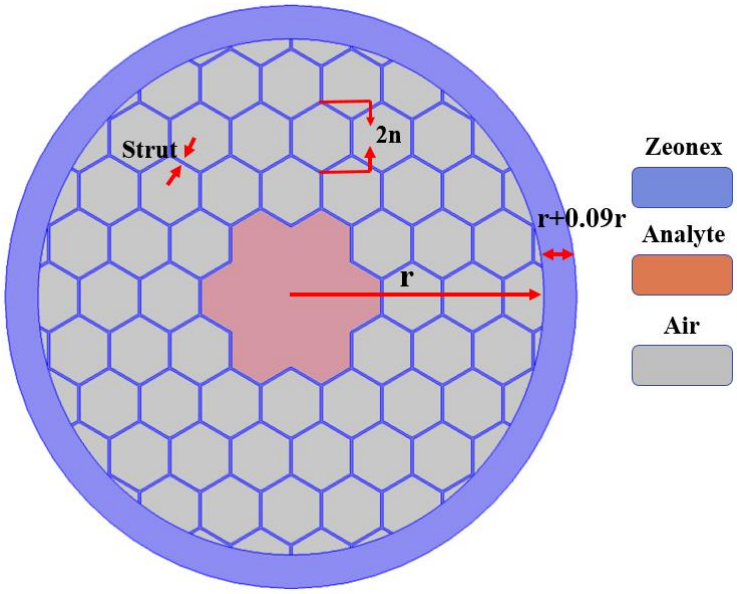

Fig. 1. *Cross-section of the HC-PCF.*

For designing an optical fiber, high heat resistance (Tg =139°C) and very low focal length change after heat and humidity exposure are required and Zeonex is a perfect fit for this kind of optical applications as it offers low moisture absorption, better transparency and higher accuracy in molding. Refractive index of Zeonex is 1.531 [38] whereas benzene, methanol and water have refractive indices of 1.4853, 1.3145 and 1.333 respectively [39].

Light can be controlled by one of the two methods in a PCF based sensor which are photonic bandgap (PBG) and the modified total internal reflection (MTIR) effect. High refractive index analytes were utilized for the proposed design, MTIR is the controlling mechanism of light for the desired sensor as it becomes effective when refractive index of the core itself becomes greater than the refractive index of the cladding [40].

The outermost part of the design is PML which takes about 5% of total radius. PML is a medium which has anisotropic and complex valued permittivity and

permeability. PML is added to the exterior of the model for absorbing all outgoing wave [41]. The core of the HC-PCF has a lower EML than standard PCF as its core is hollow and only analytes are present without any substantial material.

We have used COMSOL Multi-Physics 5.3 for our designing. It can be interface with MATLAB for programming & plotting.

Before showing our implemented designs, we would like to introduce some important parameters which act as tremendous factor for designing a fiber are described below.

8.2.1 Parameters

Table 8.1: Parameter definition

Parameters

Parameters

Name	Expression	Value	Description
n	D/4[um]	100	D/4.08165[um] for 98, D/4.16665[um] for 96
n1	D/8[um]	50	
n2	sqrt(n*n-n1*n1)	86.603	
f	3[THz]	3E12 Hz	
pcc	1.18*W	3.8383E-5 m	core pitch
porosity	0.43	0.43	
D	400[um]	4E-4 m	core diameter
d1	4[um]	4E-6 m	width of stubs
k	pi/6	0.5236	
a	cos(k)	0.86603	
b	sin(k)	0.5	
d	d1/a	4.6188E-6 m	stubs difference length
p	D/2-d	1.9538E-4 m	
r1	4.78*p*a	8.088E-4 m	
l1	r1	8.088E-4 m	length of rectangle
l2	3*l1	0.0024264 m	
u	-90	-90	
v	30	30	

8.3 Fabrication

There are several fabrication technologies available nowadays to fabricate asymmetrical shaped structures. The 3D printing and extrusion technology is able to fabricate any types of complex PCF structure including the kagome the hexagonal shape of air hole we proposed. After making filament using Zeonex, it is possible to make the preform of the structure using high resolution 3D printer and then extrude the preform using the extrusion technique [4, 42, 57]. Note that, Atakaramians et. al fabricated different complex PCF structure using extrusion technique [57]. Moreover, cubillas et al. fabricated the hexagonal shaped air hole based structure for sensing application in the optical length [Fig. 1(c), ref. 4].

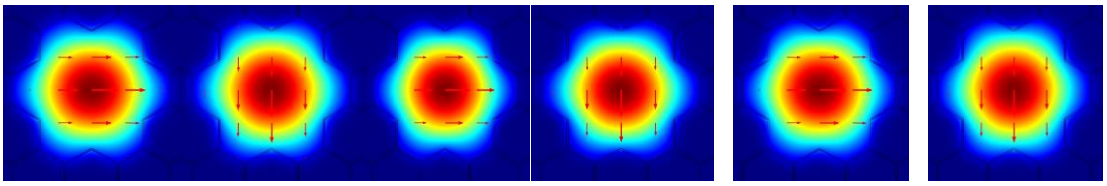

(a) (b) (c) (d) (e) (f)

Fig. 2. Power flow distribution at 3 THz frequency for (a) Methanol, x-pol, (b) Methanol, y-pol, (c) Benzene, x-pol, (d) Benzene, y-pol, (e) water, x-pol, (f) water, y-pol, keeping other design parameters optimum.

8.4 Numerical Results and Discussion

The distribution of the mode power of the proposed HC-PCF at a frequency of 3 THz is shown in Fig. 2. It can be seen that light is strongly confined for both x and y-polarization within the hollow core which is filled with the analytes (Methanol,

Benzene and Water). It is to be noted that only the fundamental modes propagate through the core.

The amount of light-interaction with matter can be calculated by the following equation [33],

$$r = \frac{n_r}{n_{eff}} \times e \tag{1}$$

Where r represents relative sensitivity, n_r and n_{eff} represents the real part of the refractive index of the analyte and effective refractive index of the guided mode respectively. e is the amount of light interaction with matter and is given by

$$e = \frac{\int_{sample} R_e \left(E_x H_y - E_y H_x \right) dxdy}{\int_{total} R_e \left(E_x H_y - E_y H_x \right) dxdy} \times 100 \tag{2}$$

Where E_x, E_y are the electric field components and H_x, H_y are the magnetic field components of the guided mode. The sensitivity of water was recorded to be 99.42% at optimum strut in x-polarization having a numerical value of 6.79 μm The effect of varying the strut value is not noticeable until magnified.

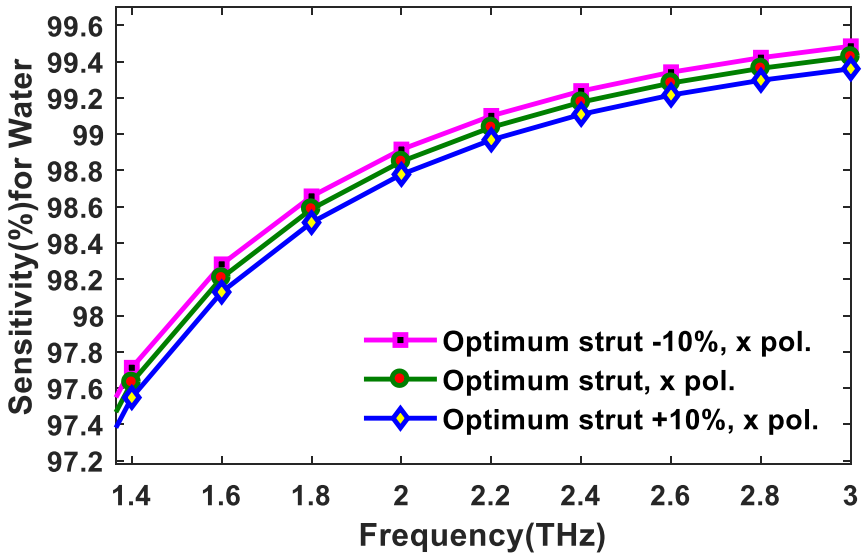

Fig. 3. Sensitivity of Water vs frequency for strut variation in x polarization.

By increasing the value of strut to 7.47 μm (+10%) the new sensitivity reduces to 99.36% and on the other hand there is a rise in sensitivity to 99.48% when the strut value is set to 6.11 μm (-10%). All these data are taken at a frequency of 3 THz.

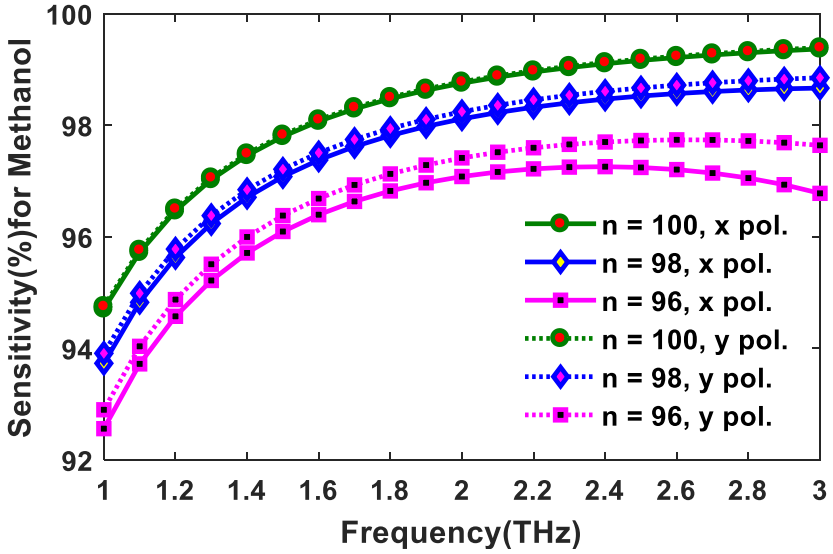

Fig. 4. Sensitivity vs frequency for Methanol at different values of n for both x and y-polarization.

Fig. 4, Fig. 5 and Fig. 6 unveils the sensitivity of methanol, benzene and water for both the orthogonal polarization and varying n. It can be seen that sensitivity increases for all the analyses with frequency. It is due to the fact that sensitivity depends on RI and the contained useful power within the core, both of which rises with frequency and as such the sensitivity is boosted. In case of methanol, at higher frequencies sensitivity is better in y-polarization than that in x-polarization. The same result is also obtained for water and in case of benzene there is not much to differentiate. In the proposed structure a stronger confinement of light occurs in the y-polarization and so y-pol is chosen as the optimum condition.

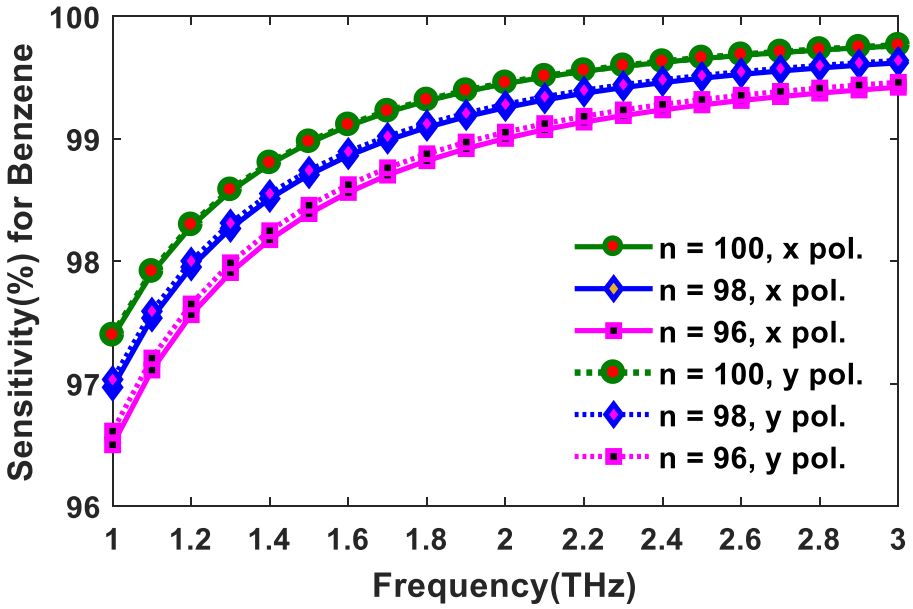

Fig. 5. Sensitivity vs frequency for Benzene at different values of n for both x and y-polarization.

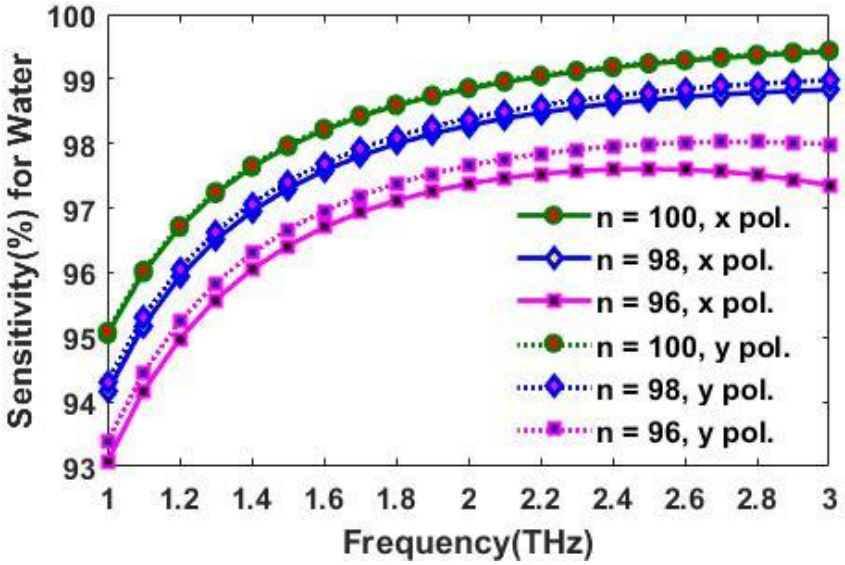

Fig. 6. Sensitivity vs frequency for Water at different values of n for both x and y-polarization.

A closer look at the figures reveals that sensitivity slightly decreases after 2.5 THz frequency for water and methanol. Although core power fraction is supposed to escalate with frequency but at a particular frequency it reaches its peak and further increment of frequency results some of the useful power to penetrate into the cladding region and thus the core power attenuates. This phenomenon causes the sensitivity to drop after a particular frequency. In case of x-polarization the sensitivity is as high as 99.37%, 99.75% and 99.42% at 3 THz frequency and n =100 for methanol, benzene and water respectively. But at optimum condition that is in y-pol the sensitivity is 99.39%, 99.76% and 99.44% at 3 THz frequency and n = 100 for methanol, benzene and water respectively. It can be observed that the sensitivity is high for both the orthogonal modes and it is so far the best sensitivity obtained for the mentioned analyses to the best of our knowledge.

Fig. 7 shows a comparison of sensitivity for different analytes. The recorded sensitivity is comparatively low at lower frequencies but it rises rapidly with frequency. Among the three analytes, the relative sensitivity is the best for benzene because it has a high refractive index that causes the lights interacts more strongly with the analyte.

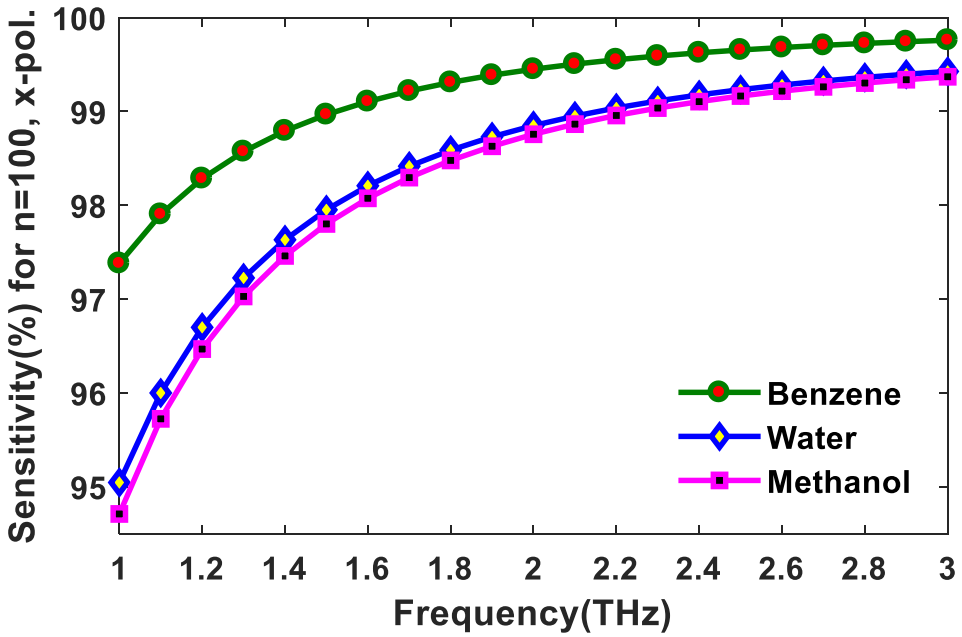

Fig. 7. Comparison of sensitivity for different analyses at optimum design conditions.

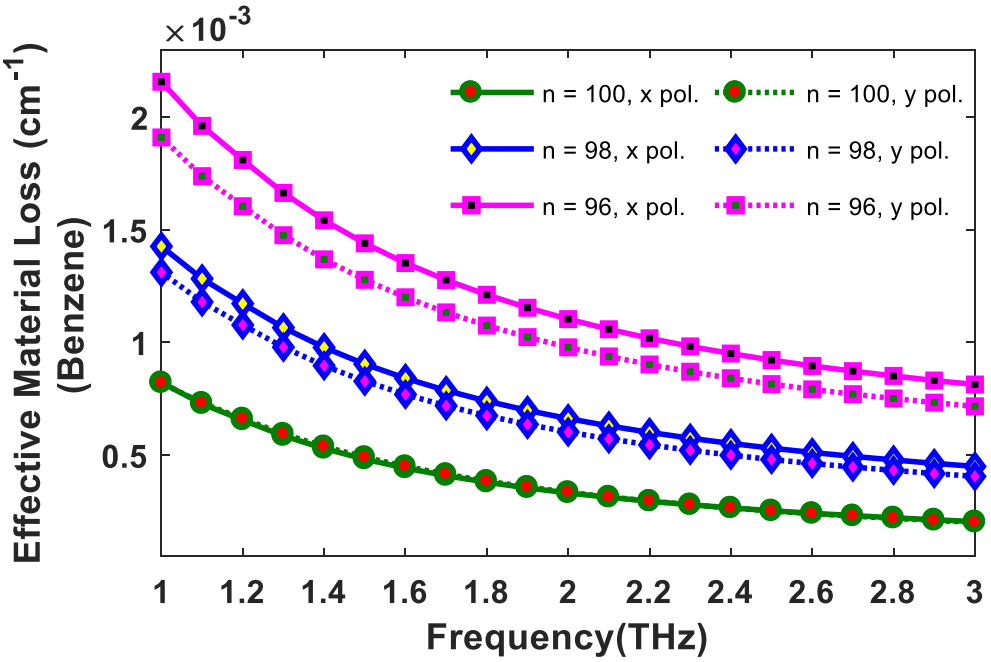

Fig. 8. Effective material loss of Benzene with respect to frequency for varying n at different polarization modes.

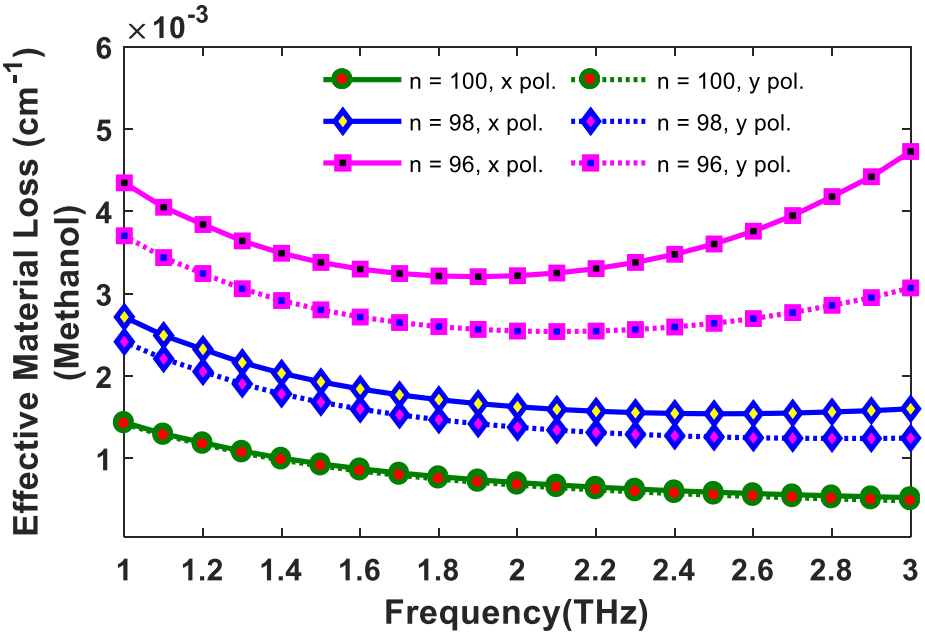

Fig. 9. Effective material loss of Methanol with respect to frequency for varying n at different polarization modes.

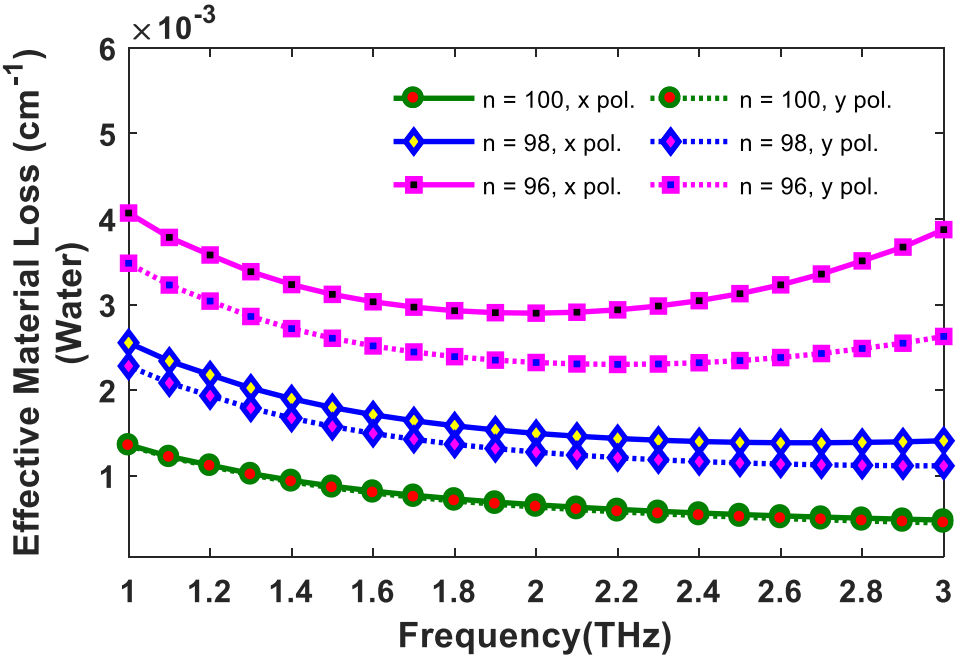

Fig. 10. Effective material loss of Water with respect to frequency for varying n at different polarization modes.

EML is one of the factors which limit the performance of a waveguide. This property of a PCF can be calculated by

$$\alpha_{eff} = \sqrt{\frac{\varepsilon_0}{\mu_0}} \left(\sqrt{\frac{\int_{mat} n_{mat} |\mathrm{E}|^2 \alpha_{mat} dA}{\left| \int_{all} S_z dA \right|}} \right) \tag{3}$$

where ε_0 and μ_0 designate permittivity and permeability in vacuum respectively, α_{mat} is the bulk material absorption loss, n_{mat} represents the refractive index , E indicates the E-field mode distribution and S_z implies the pointing vector in the z-direction. The gradual change of EML with frequency can be observed from Fig. 8,

Fig. 9 and Fig. 10 where EML is found to attenuate with frequency. This can be explained by the fact that a rise in frequency decreases the confinement loss (Fig. 11) which signifies that light pulses are more tightly confined within the core rather than the cladding. Since the proposed PCF is void of any bulk material within the core, the EML shrinks. It can be explained by the fact that, after a particular frequency, the core becomes insufficient to confine all the useful power which then penetrates into the cladding resulting in a small escalation in EML. The EML response of all the analytes, at optimum design conditions, are respectively 0.0005 cm^{-1}, 0.0002 cm^{-1} and 0.0004 cm^{-1} for methanol, benzene and water which are still one of the lowest EMLs ever recorded [43-46].

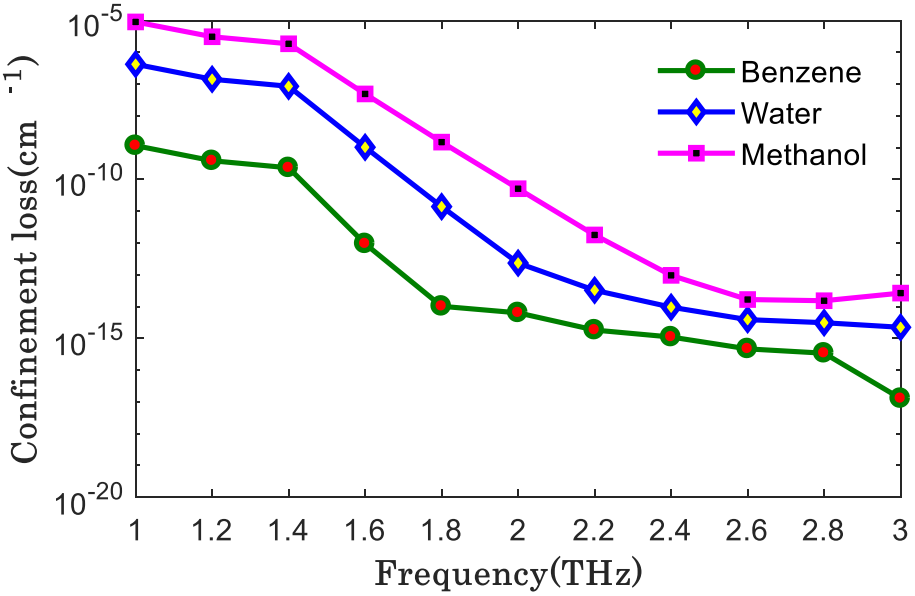

Fig. 11. Confinement loss vs frequency for different analytes.

Confinement loss is a vital factor which is responsible for ensuring a better propagation length for terahertz PCF [36]. This parameter can be calculated by

$$L_c = \frac{4\pi f}{c}\,\mathrm{Im}\left(n_{eff}\right),\ \mathrm{cm}^{-1} \tag{4}$$

where f and c represents the frequency and speed of light in vacuum respectively and $\mathrm{Im}\left(n_{eff}\right)$ stands for the imaginary part of the refractive index. Fig. 11 reflects the outcome of equation (4) for methanol, benzene and water. For all the analytes confinement loss is seen to attenuate with frequency as expected because higher frequency causes a better confinement of light within the hollow core region.

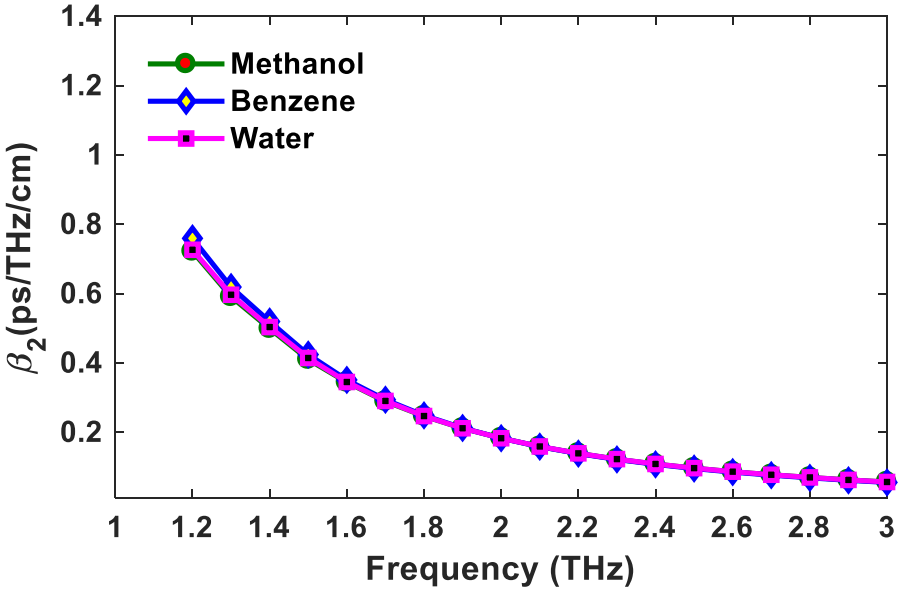

Fig. 12. Dispersion variation as a function of frequency for different analytes.

The dispersion relation of the proposed structure with frequency is depicted in Fig. 12 which follows the relation

$$\beta_2 = \frac{2}{c}\frac{dn_{eff}}{d\omega} + \frac{\omega}{c}\frac{d^2 n_{eff}}{d\omega^2} \tag{5}$$

where c stands for the speed of light in vacuum, n_{eff} is the effective refractive index of the core and ω is the angular frequency. It is observed that β_2 is almost identical for methanol, benzene and water and it is as low as 0.0562 ps/THz/cm, 0.055 ps/THz/cm and 0.0563 ps/THz/cm respectively. Further dispersion is essentially flat from 1.8 THz to 3 THz. The significance of flat dispersion lies in its capability of reducing pulse broadening and thereby decreasing the probability of bit error rate.

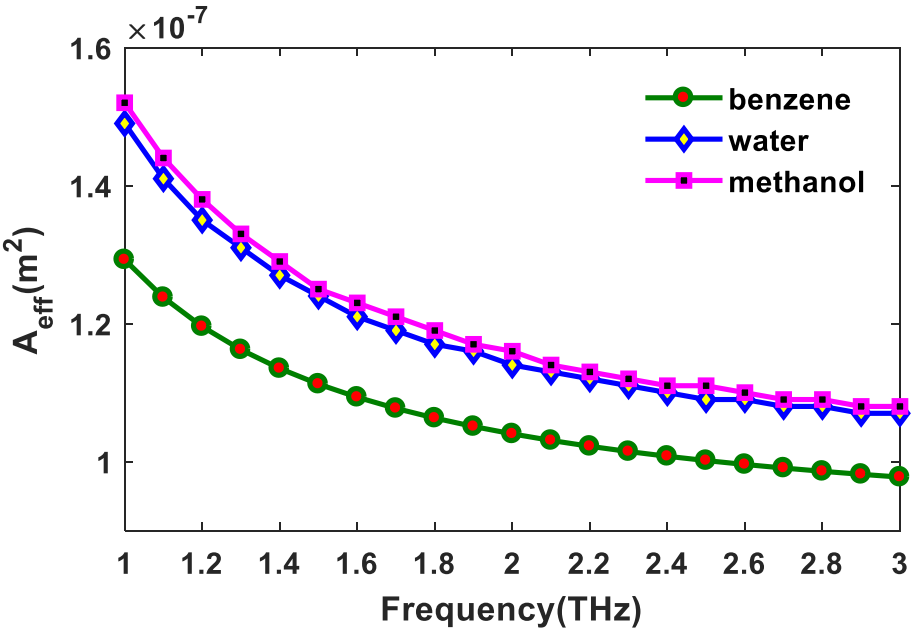

Fig. 13. Effective area as a function of frequency for different analytes at=100.

The area where matter interacts with light intensities is defined as effective area and Fig. 13 demonstrates its gradual change with changing frequency. Effective area can be calculated by

$$A_{eff} = \frac{\left[\int I(r) r dr\right]^2}{\left[\int I^2(r) dr\right]^2} \tag{6}$$

Where $I(r)$ is the transverse electric intensity distribution and it follows the relation $I(r)=|E_t|^2$. As frequency increases the amount of light confining within the core region decreases which leads the effective area to diminish with frequency. Though the effective area is only 9.78 μm^2 for benzene, it raises to 10.7 μm^2 and 10.8 μm^2 for water and methanol respectively at optimum design conditions.

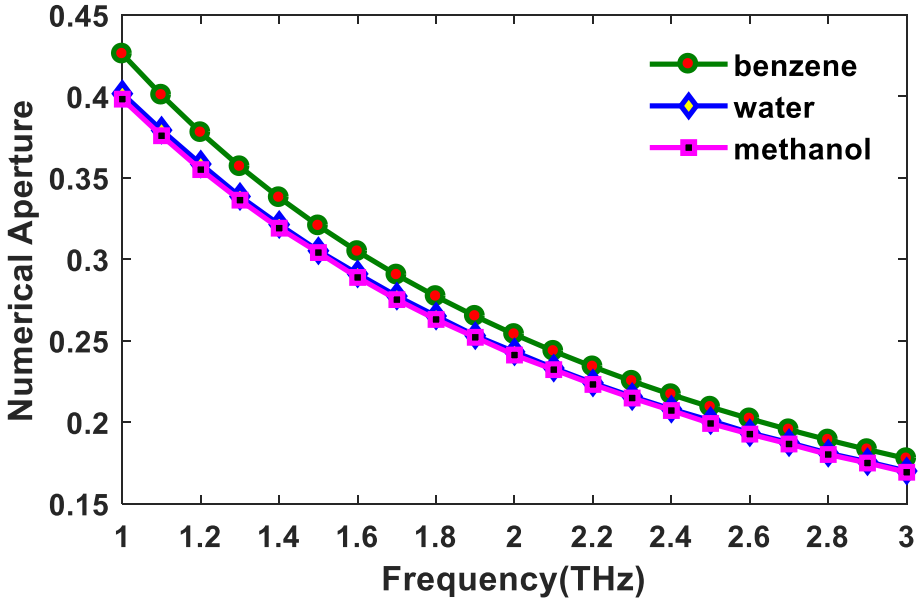

Fig. 14. Frequency response of numerical aperture for different analytes.

Numerical aperture is another significant feature of any PCF which surprisingly a lot of previous sensors neglect to mention. The numerical aperture follows the relation

$$NA=\frac{1}{\sqrt{1+\frac{\pi A_{eff} f^2}{c^2}}}$$

The numerical aperture of the hollow core photonic crystal fiber is 0.1776, 0.17 and 0.1692 for benzene, water and methanol respectively at optimum conditions. It is to

be noted that numerical aperture depends on the difference between the RI of the core and cladding as can be realized from the equation. The application of a wide numerical aperture is in the field of sensing and optical tomography applications.

TABLE I

COMPARISON OF CHARACTERISTICS BETWEEN THE PROPOSED SENSOR AND PRIOR SENSORS FOR CHEMICAL ANALYTE DETECTION

Ref.	Operating region	Water		Benzene	
		Sensitivity (%)	EML (cm^{-1})	Sensitivity (%)	EML (cm^{-1})
[55]	1.33μm	48.19	-	55.56	-
[56]	1.33μm	60.57	-	61.82	-
[33]	1.6 THz	85.6%	-	85.9%	-
[40]	1.4 THz	96.69%	0.0034	97.2%	0.0036
This paper	3 THz	99.44%	0.0004	99.76%	0.0002

Table I clearly shows the comparison of the proposed novel structure with the prior designs and it clearly displays a promising outcome in consideration relative sensitivity and losses.

CHAPTER 9

CONCLUSION

In this work a novel structure is considered which consists of a hexagonal symmetrical cladding with a hollow core that promises to play a very significant role in the field of sensing applications. The study covers a wide range of 2 THz (1 THz – 3 THz). Zeonex has been used as the background material and the results display a sensitivity of 99.39%, 99.76% and 99.44% for methanol, benzene and water respectively at optimum conditions. Besides the work also analyses the other important characteristics like effective area, numerical aperture, effective material loss, confinement loss and dispersion. The outcomes of all these properties signify very competitive values with respect to the other structures but overcoming all other proposed designs so far in the field of sensitivity. Besides the proposed structure contains a symmetrical cladding with uniform hexagonal structures distributed in a total of 3 rows which ensures almost no complexity while fabrication. Thus it can be said that this novel structure containing a hexagonal cladding will add a new dimension to the future researchers for enriching the sensing applications in the terahertz region.

9.1 Drawbacks and Future Proposal

An immensely lower effective material loss, notably marginal core power fraction, less confinement loss and near zero ultra-flat dispersion has been introduced in our proposed design. In our proposed design, single mode properties has also been satisfied and designed for THz wave guidance. For the first time Octagonal cladding and rotate hexagonal core has been introduced which helps us to reduce the effective material loss and preferably for a margin of core power fraction. Besides, higher air filling fraction and unique arrangement of five rings in the cladding helps to decrease the confinement loss. The primary implication of our proposed structure is its simplicity and loss reduction. Our proposed design contains attractive guiding properties which will be significant for THz wave application. For long distance communication of THz signal, our proposed design can be used relevantly.

The main drawback of our proposed design is power fraction can further be increased & EML can further be decreased. Still the accumulated result is satisfactory & can be developed in future for practical purpose.

So the future goal should be developing a fabrication process for this accumulated design which is efficient & easy so that worldwide it can be adopted. Furthermore, simulations should be continued for new designs so that low EML& high power fraction design can be adopted & fabricated practically.

REFERENCES

1. O. Sidek and M. H. B. Afzal, "A review paper on fiber-optic sensors and application of pDMS materials for enhanced performance," in Business, Engineering and Industrial Applications (ISBEIA), 2011 IEEE Symposium on, (IEEE, 2011), 458-463.
2. P. Yeh, A. Yariv, and E. Marom, "Theory of Bragg fiber," JOSA 68, 1196-1201 (1978).
3. J. Knight, T. Birks, P. S. J. Russell, and D. Atkin, "All-silica single-mode optical fiber with photonic crystal cladding," Optics letters 21, 1547-1549 (1996).
4. A. M. Cubillas, S. Unterkofler, T. G. Euser, B. J. Etzold, A. C. Jones, P. J. Sadler, P. Wasserscheid, and P. S. J. Russell, "Photonic crystal fibres for chemical sensing and photochemistry," Chemical Society Reviews 42, 8629-8648 (2013).
5. P. Blanchard, J. Burnett, G. Erry, A. Greenaway, P. Harrison, B. Mangan, J. Knight, P. S. J. Russell, M. Gander, and R. McBride, "Two-dimensional bend sensing with a single, multi-core optical fibre," Smart materials and structures 9, 132 (2000).
6. H. V. Thakur, S. M. Nalawade, Y. Saxena, and K. Grattan, "All-fiber embedded PM-PCF vibration sensor for Structural Health Monitoring of composite," Sensors and Actuators A: Physical 167, 204-212 (2011).
7. G. Rajan, M. Ramakrishnan, Y. Semenova, A. Domanski, A. Boczkowska, T. Wolinski, and G. Farrell, "Analysis of vibration measurements in a composite material using an embedded PM-PCF polarimetric sensor and an FBG sensor," IEEE Sensors Journal 12, 1365-1371 (2012).
8. W. Bock, J. Chen, P. Mikulic, T. Eftimov, and M. Korwin-Pawlowski, "Pressure sensing using periodically tapered long-period gratings written in photonic crystal fibres," Measurement Science and Technology 18, 3098 (2007).
9. L. Zou, X. Bao, S. Afshar, and L. Chen, "Dependence of the Brillouin frequency shift on strain and temperature in a photonic crystal fiber," Optics letters 29, 1485-1487 (2004).
10. J. Broeng, T. Søndergaard, S. E. Barkou, P. M. Barbeito, and A. Bjarklev, "Waveguidance by the photonic bandgap effect in optical fibres," Journal of Optics A: Pure and Applied Optics 1, 477 (1999).
11. M. Foroni, D. Passaro, F. Poli, A. Cucinotta, S. Selleri, J. Lægsgaard, and A. Bjarklev, "Confinement loss spectral behavior in hollow-core Bragg fibers," Optics letters 32, 3164-3166 (2007).
12. A. L. Cruz, C. Cordeiro, and M. A. Franco, "3D Printed Hollow-Core Terahertz Fibers," Fibers 6, 43 (2018).
13. R. Cregan, B. Mangan, J. Knight, T. Birks, P. S. J. Russell, P. Roberts, and D. Allan, "Single-mode photonic band gap guidance of light in air," science 285, 1537-1539 (1999).

14. G. Humbert, J. Knight, G. Bouwmans, P. S. J. Russell, D. Williams, P. Roberts, and B. Mangan, "Hollow core photonic crystal fibers for beam delivery," Optics express 12, 1477-1484 (2004).
15. F. Gérôme, K. Cook, A. George, W. Wadsworth, and J. Knight, "Delivery of sub-100fs pulses through 8m of hollow-core fiber using soliton compression," Optics express 15, 7126-7131 (2007).
16. F. Gérôme, P. Dupriez, J. Clowes, J. Knight, and W. Wadsworth, "High power tunable femtosecond soliton source using hollow-core photonic bandgap fiber, and its use for frequency doubling," Optics express 16, 2381-2386 (2008).
17. A. Urich, R. Maier, F. Yu, J. C. Knight, D. Hand, and J. Shephard, "Flexible delivery of Er: YAG radiation at 2.94 μm with negative curvature silica glass fibers: a new solution for minimally invasive surgical procedures," Biomedical optics express 4, 193-205 (2013).
18. J. Anthony, R. Leonhardt, S. G. Leon-Saval, and A. Argyros, "THz propagation in kagome hollow-core microstructured fibers," Optics express 19, 18470-18478 (2011).
19. A. Cubillas, M. Silva-Lopez, J. Lazaro, O. Conde, M. N. Petrovich, and J. M. Lopez-Higuera, "Methane detection at 1670-nm band using a hollow-core photonic bandgap fiber and a multiline algorithm," Optics Express 15, 17570-17576 (2007).
20. A. Cubillas, J. Lazaro, M. Silva-Lopez, O. Conde, M. Petrovich, and J. Lopez-Higuera, "Methane sensing at 1300 nm band with hollow-core photonic bandgap fibre as gas cell," Electronics Letters 44, 403-405 (2008).
21. J. B. Jensen, L. H. Pedersen, P. E. Hoiby, L. B. Nielsen, T. P. Hansen, J. R. Folkenberg, J. Riishede, D. Noordegraaf, K. Nielsen, and A. Carlsen, "Photonic crystal fiber based evanescent-wave sensor for detection of biomolecules in aqueous solutions," Optics letters 29, 1974-1976 (2004).
22. N. Burani and J. Lægsgaard, "Perturbative modeling of Bragg-grating-based biosensors in photonic-crystal fibers," JOSA B 22, 2487-2493 (2005).
23. L. Rindorf, J. B. Jensen, M. Dufva, L. H. Pedersen, P. E. Høiby, and O. Bang, "Photonic crystal fiber long-period gratings for biochemical sensing," Optics Express 14, 8224-8231 (2006).
24. R. A. Rinsky, A. B. Smith, R. Hornung, T. G. Filloon, R. J. Young, A. H. Okun, and P. J. Landrigan, "Benzene and leukemia," New England journal of medicine 316, 1044-1050 (1987).
25. R. B. Hayes, M. Dosemeci, S. Wacholder, L. B. Travis, N. Rothman, R. N. Hoover, M. S. Linet, S.-N. Yin, G.-L. Li, and C.-Y. Li, "Benzene and the dose-related incidence of hematologic neoplasms in China," Journal of the National Cancer Institute 89, 1065-1071 (1997).
26. E. Lynge, A. Andersen, R. Nilsson, L. Barlow, E. Pukkala, R. Nordlinder, P. Boffetta, P. Grandjean, P. Heikkiia, and L.-G. Horte, "Risk of cancer and exposure to gasoline vapors," American journal of epidemiology 145, 449-458 (1997).

27. O. S. Wolfbeis, "Fiber-optic chemical sensors and biosensors," Analytical chemistry 80, 4269-4283 (2008).
28. M. H. B. Afzal, "Introduction to fibre-optic sensing system and practical applications in water quality management," in Computing, Communications and Networking Technologies (ICCCNT), 2013 Fourth International Conference on, (IEEE, 2013), 1-9.
29. K. Fidanboylu and H. Efendioglu, "Fiber optic sensors and their applications," in 5th International Advanced Technologies Symposium (IATS'09), 2009),
30. U. D. o. Health and H. Services, "Hazardous substances data bank (HSDB, online database)," National Toxicology Information Program, National Library of Medicine, Bethesda, MD (1993).
31. U. D. o. Health and H. Services, "Registry of toxic effects of chemical substances (RTECS, online database)," National Toxicology Information Program, National Library of Medicine, Bethesda, MD 4(1993).
32. R. P. Pohanish, Sittig's handbook of toxic and hazardous chemicals and carcinogens (William Andrew, 2017).
33. M. S. Islam, J. Sultana, K. Ahmed, M. R. Islam, A. Dinovitser, B. W.-H. Ng, and D. Abbott, "A novel approach for spectroscopic chemical identification using photonic crystal fiber in the terahertz regime," IEEE Sensors Journal 18, 575-582 (2018).
34. K. Ahmed, M. I. Islam, B. K. Paul, M. S. Islam, S. Sen, S. Chowdhury, M. S. Uddin, S. Asaduzzaman, and A. N. Bahar, "Effect of photonic crystal fiber background materials in sensing and communication applications," Materials Discovery 7, 8-14 (2017).
35. M. Goto, A. Quema, H. Takahashi, S. Ono, and N. Sarukura, "Teflon photonic crystal fiber as terahertz waveguide," Japanese Journal of Applied Physics 43, L317 (2004).
36. M. S. Islam, J. Sultana, S. Rana, M. R. Islam, M. Faisal, S. F. Kaijage, and D. Abbott, "Extremely low material loss and dispersion flattened TOPAS based circular porous fiber for long distance terahertz wave transmission," Optical Fiber Technology 34, 6-11 (2017).
37. J. Anthony, R. Leonhardt, A. Argyros, and M. C. Large, "Characterization of a microstructured Zeonex terahertz fiber," JOSA B 28, 1013-1018 (2011).
38. G. Emiliyanov, J. B. Jensen, O. Bang, P. E. Hoiby, L. H. Pedersen, E. M. Kjær, and L. Lindvold, "Localized biosensing with TOPAS microstructured polymer optical fiber: Erratum," Optics letters 32, 460-462 (2007).
39. M. Polyanskiy, "RefractiveIndex. INFO-Refractive index database," RefractiveIndex. INFO,[Online]. Available: http://refractiveindex. info/.[Accessed 25 Jan 2016] (2018).
40. M. S. Islam, J. Sultana, A. A. Rifat, A. Dinovitser, B. W.-H. Ng, and D. Abbott, "Terahertz sensing in a hollow core photonic crystal fiber," IEEE Sensors Journal 18, 4073-4080 (2018).
41. W. Frei, "Using perfectly matched layers and scattering boundary conditions for wave electromagnetics problems," URL https://www. comsol. com/blogs/usingperfectly-matched-layers-and-scattering-boundary-conditions-for-waveelectromagnetics-problems/.(referenced 1.6. 2017) (2015).

42. H. Ebendorff-Heidepriem, J. Schuppich, A. Dowler, L. Lima-Marques, and T. M. Monro, "3D-printed extrusion dies: a versatile approach to optical material processing," Optical Materials Express 4, 1494-1504 (2014).
43. R. Islam, M. S. Habib, G. Hasanuzzaman, S. Rana, M. A. Sadath, and C. Markos, "A novel low-loss diamond-core porous fiber for polarization maintaining terahertz transmission," IEEE Photon. Technol. Lett. 28, 1537-1540 (2016).
44. M. Cho, J. Kim, H. Park, Y. Han, K. Moon, E. Jung, and H. Han, "Highly birefringent terahertz polarization maintaining plastic photonic crystal fibers," Optics Express 16, 7-12 (2008).
45. S. Atakaramians, S. Afshar, B. M. Fischer, D. Abbott, and T. M. Monro, "Low loss, low dispersion and highly birefringent terahertz porous fibers," Optics communications 282, 36-38 (2009).
46. H. Chen, D. Chen, and Z. Hong, "Squeezed lattice elliptical-hole terahertz fiber with high birefringence," Applied optics 48, 3943-3947 (2009).
47. G. Emiliyanov, P. E. Høiby, L. H. Pedersen, and O. Bang, "Selective serial multi-antibody biosensing with TOPAS microstructured polymer optical fibers," Sensors 13, 3242-3251 (2013).
48. J. Sultana, M. S. Islam, J. Atai, M. R. Islam, and D. Abbott, "Near-zero dispersion flattened, low-loss porous-core waveguide design for terahertz signal transmission," Optical Engineering 56, 076114 (2017).
49. S. Asaduzzaman, K. Ahmed, T. Bhuiyan, and T. Farah, "Hybrid photonic crystal fiber in chemical sensing," SpringerPlus 5, 748 (2016).
50. K. Lee and S. A. Asher, "Photonic crystal chemical sensors: pH and ionic strength," Journal of the American Chemical Society 122, 9534-9537 (2000).
51. H. Ademgil and S. Haxha, "PCF based sensor with high sensitivity, high birefringence and low confinement losses for liquid analyte sensing applications," Sensors 15, 31833-31842 (2015).
52. B. K. Paul, M. S. Islam, K. Ahmed, and S. Asaduzzaman, "Alcohol sensing over O+ E+ S+ C+ L+ U transmission band based on porous cored octagonal photonic crystal fiber," Photonic Sensors 7, 123-130 (2017).
53. S. Asaduzzaman and K. Ahmed, "Microarray-core based circular photonic crystal fiber for high chemical sensing capacity with low confinement loss," Optica Applicata 47(2017).
54. S. Chowdhury, S. Sen, K. Ahmed, and S. Asaduzzaman, "Design of highly sensible porous shaped photonic crystal fiber with strong confinement field for optical sensing," Optik-International Journal for Light and Electron Optics 142, 541-549 (2017).
55. M. S. Islam, B. K. Paul, K. Ahmed, S. Asaduzzaman, M. I. Islam, S. Chowdhury, S. Sen, and A. N. Bahar, "Liquid-infiltrated photonic crystal fiber for sensing purpose: design and analysis," Alexandria Engineering Journal (2017).
56. S. Chowdhury, S. Sen, K. Ahmed, B. K. Paul, M. B. A. Miah, S. Asaduzzaman, M. S. Islam, and M. I. Islam, "Porous shaped photonic crystal fiber with strong confinement field

in sensing applications: design and analysis," Sensing and Bio-Sensing Research 13, 63-69 (2017)

57. Shaghik Atakaramians, Shahraam Afshar V., Heike Ebendorff-Heidepriem, Michael Nagel, Bernd M. Fischer, Derek Abbott, and Tanya M. Monro, "THz porous fibers: design, fabrication and experimental characterization," Opt. Express 17, 14053-14062 (2009).
58. J. C. Travers *et al.*, "Ultrafast nonlinear optics in gas-filled hollow-core photonic crystal fibers," *J. Opt. Soc. Amer. B*, vol. 28, no. 12, pp. A11–A26, 2011.
59. M. A. Hossain and Y. Namihira, "Light source design using Kagomelattice hollow core photonic crystal fibers," *Opt. Rev.*, vol. 21, no. 5, pp. 490–495, 2014.
60. J. Anthony, R. Leonhardt, S. G. Leon-Saval, and A. Argyros, "THz propagation in kagome hollow-core microstructured fibers," *Opt. Exp.*, vol. 19, no. 19, pp. 18470–18478, 2011.
61. G. K. M. Hasanuzzaman, M. Selim Habib, S. M. Abdur Razzak, M. A. Hossain and Y. Namihira, "Low Loss Single-Mode Porous-Core Kagome Photonic Crystal Fiber for THz Wave Guidance," *Journal of Lightwave Technology*, vol. 33, no. 19, pp. 4027-4031, 1 Oct.1, 2015
62. Md. Shariful Islam, Mohammad Faisal, and S. M. Abdur Razzak, "Extremely low loss porous-core photonic crystal fiber with ultra-flat dispersion in terahertz regime," J. Opt. Soc. Am. B 34, 1747-1754 (2017).